

MASTERS DISSERTATION

**MULTI-UNCERTAINTY ANALYSIS OF SPHERE-TO-FLAT
INDENTATION TESTS OF PC/ABS BLENDS**

**BY
THIERRE LORENZO AMARAL**

**UNIVERSITY OF BRASÍLIA
FACULTY OF TECHNOLOGY
DEPARTMENT OF MECHANICAL ENGINEERING**

UNIVERSITY OF BRASÍLIA
FACULTY OF TECHNOLOGY
DEPARTMENT OF MECHANICAL ENGINEERING

MASTERS DISSERTATION

**MULTI-UNCERTAINTY ANALYSIS OF SPHERE-TO-FLAT
INDENTATION TESTS OF PC/ABS BLENDS**

A Dissertation Presented to the
Department of Mechanical Engineering

by
Thierre Lorenzo Amaral

In Partial Fulfillment
of the Requirements for the Degree of
Master in Mechanical Science

Supervisor: Prof. Thiago de Carvalho Rodrigues Doca, Ph.D.

**PUBLICAÇÃO ENM.DM - XXX/AAAA
BRASÍLIA-DF, 26 DE JANEIRO DE 2021.**

UNIVERSITY OF BRASÍLIA
FACULTY OF TECHNOLOGY
DEPARTMENT OF MECHANICAL ENGINEERING

MASTERS DISSERTATION

**MULTI-UNCERTAINTY ANALYSIS OF SPHERE-TO-FLAT
INDENTATION TESTS OF PC/ABS BLENDS**

Approved by:

Prof. Thiago de Carvalho Rodrigues Doca, Ph.D. - Supervisor
ENM-UnB

Prof. Jorge Luiz de Almeida Ferreira, D.Sc. - Internal Examiner
ENM-UnB

Prof. Washington Martins da Silva Júnior, D.Sc. - External Examiner
FEMEC-UFU

BRASÍLIA, 26 DE JANEIRO DE 2021.

FICHA CATALOGRÁFICA

THIERRE LORENZO AMARAL

MULTI-UNCERTAINTY ANALYSIS OF SPHERE-TO-FLAT INDENTATION TESTS OF PC/ABS BLENDS.

2021xv, 83p., 201x297 mm

(ENM/FT/UnB, Mestre, Engenharia Mecânica, 2021)

Dissertação de Mestrado - Universidade de Brasília - Faculdade de Tecnologia

Departamento de Engenharia Mecânica

REFERÊNCIA BIBLIOGRÁFICA

THIERRE LORENZO AMARAL (2021) Multi-Uncertainty Analysis of Sphere-to-Flat Indentation Tests of PC/ABS Blends. Dissertação de Mestrado em Engenharia Mecânica, Publicação xxx/AAAA, Departamento de Engenharia Mecânica, Universidade de Brasília, Brasília, DF, 83p.

CESSÃO DE DIREITOS

AUTOR: Thierre Lorenzo Amaral

TÍTULO: Multi-Uncertainty Analysis of Sphere-to-Flat Indentation Tests of PC/ABS Blends.

GRAU: Mestre

ANO: 2021

É concedida à Universidade de Brasília permissão para reproduzir cópias desta dissertação de Mestrado e para emprestar ou vender tais cópias somente para propósitos acadêmicos e científicos. O autor se reserva a outros direitos de publicação e nenhuma parte desta dissertação de Mestrado pode ser reproduzida sem a autorização por escrito do autor.

Thierre Lorenzo Amaral
thierrelorenzo@gmail.com

TABLE OF CONTENTS

| | | |
|----------|--|-----------|
| 1 | INTRODUCTION | 1 |
| 1.1 | BACKGROUND AND MOTIVATION | 1 |
| 1.2 | RESEARCH GOALS | 3 |
| 1.3 | OUTLINE | 3 |
| 2 | CONCEPTS | 5 |
| 2.1 | POLYMERS | 5 |
| 2.1.1 | POLYCARBONATE (PC) | 6 |
| 2.1.2 | ACRYLONITRILE-BUTADINE-STYRENE (ABS) | 6 |
| 2.1.3 | PC/ABS BLENDS | 7 |
| 2.2 | CONTACT MECHANICS | 8 |
| 2.2.1 | SPHERE-TO-FLAT HERTZIAN SOLUTION | 8 |
| 2.2.2 | NON-LINEAR MATERIAL BEHAVIOR | 11 |
| 2.3 | COMPRESSION TESTS | 13 |
| 2.3.1 | INDENTATION TESTS | 14 |
| 2.3.2 | HARDNESS TESTS | 14 |
| 2.3.3 | STANDARDIZED TESTS | 15 |
| 2.4 | MULTI-UNCERTAINTY | 18 |
| 3 | MATERIALS AND METHODS | 19 |
| 3.1 | EXPERIMENTAL SETUP | 19 |
| 3.1.1 | EQUIPMENT | 19 |
| 3.1.2 | SAMPLES | 23 |
| 3.2 | TESTING PROCEDURE | 24 |

| | | |
|----------|---|-----------|
| 3.3 | UNCERTAINTY ANALYSIS | 28 |
| 3.3.1 | MANUFACTURE ERRORS | 28 |
| 3.3.2 | REPEATABILITY | 29 |
| 3.3.3 | MEASUREMENT UNCERTAINTIES | 30 |
| 3.4 | DATA TREATMENT | 35 |
| 4 | RESULTS AND DISCUSSION | 38 |
| 4.1 | HERTZIAN SOLUTION | 38 |
| 4.2 | INDENTATION RESULTS | 40 |
| 4.2.1 | DATA TREATMENT | 40 |
| 4.2.2 | LOAD-DISPLACEMENT CURVES | 40 |
| 4.3 | MICROSCOPIC INSPECTION | 42 |
| 4.4 | HARDNESS RESULTS | 47 |
| 4.5 | UNCERTAINTIES | 48 |
| 4.5.1 | LOAD | 49 |
| 4.5.2 | INDENTATION DIAMETER | 50 |
| 4.5.3 | INDENTATION DEPTH | 51 |
| 4.6 | AVERAGE MATERIAL BEHAVIOR | 54 |
| 4.6.1 | REGRESSION CURVES | 54 |
| 4.6.2 | RESIDUALS ANALYSIS | 57 |
| 5 | FINAL REMARKS | 59 |
| 5.1 | CONCLUSIONS | 59 |
| 5.2 | FUTURE WORKS | 60 |
| | REFERENCES | 62 |

LIST OF FIGURES

| | | |
|------|--|----|
| 1.1 | Polymer products manufactured by CODEPLAS®, extracted from [1]. | 2 |
| 2.1 | Contact geometry of non-conforming solids under normal compressive load [13]. | 9 |
| 2.2 | Representation of stress-strain curve of a glassy polymer, adapted from [22,23]. | 12 |
| 2.3 | Compression test with a spherical-seated bearing block [27]. | 13 |
| 2.4 | Principle of Brinell hardness tests [41]. | 17 |
| 3.1 | MTS Landmark®370 test machine with crosshead-mounted actuation [47]. | 21 |
| 3.2 | Sample holder device [3]. | 22 |
| 3.3 | (a) Hemispherical tip indenter and (b) dimensions in mm | 22 |
| 3.4 | Thickness comparison of PC samples. | 24 |
| 3.5 | Surface finish of PC samples. | 24 |
| 3.6 | Hardness testing devices. | 25 |
| 3.7 | Test machine and components: 1) Crosshead, 2) Upper Collet-Grip, 3) Bottom Collet-Grip, 4) Load Transducer, 5) Indenter, 6) Holder Device. | 25 |
| 3.8 | Sample positioning on the confocal microscope. | 26 |
| 3.9 | Stitched images of indentation marks on ABS samples (Load, Magnification). | 27 |
| 3.10 | 2D profiles of indentation marks on ABS samples. | 27 |
| 3.11 | Molding cycle components, extracted from [57]. | 28 |
| 3.12 | Manufacture errors in PC samples. | 29 |
| 3.13 | Example of an approved indenter tip. | 30 |
| 3.14 | Uncertainty analysis flowchart. | 31 |
| 3.15 | Uncertainties flowchart for the load. | 32 |
| 3.16 | Uncertainties flowchart for the load transducer. | 32 |
| 3.17 | Uncertainties flowchart for the static testing machine. | 33 |

| | | |
|------|---|----|
| 3.18 | Uncertainties flowchart for the indentation diameter and depth. | 34 |
| 3.19 | Uncertainties flowchart for the confocal microscope. | 34 |
| 3.20 | Raw data example for a PC/ABS 70:30 test at 2kN. | 36 |
| 3.21 | Noise handling example for a PC/ABS 70:30 test at 2kN. | 37 |
| 3.22 | (a) Data sampling and (b) final data examples for a PC/ABS 70:30 test at 2kN. | 37 |
| | | |
| 4.1 | Stresses along the axis of symmetry for $\nu = 0.35$ | 39 |
| 4.2 | Load-displacement curves collected during indentation tests. | 41 |
| 4.3 | Whitened area at the bottom surface of ABS samples. | 41 |
| 4.4 | Indentation marks on ABS samples. | 42 |
| 4.5 | Averaged measurements for indentation diameter. | 43 |
| 4.6 | Grouped results for indentation diameter. | 44 |
| 4.7 | Averaged measurements for indentation depth. | 45 |
| 4.8 | Grouped results for indentation depth. | 45 |
| 4.9 | Indentation displacement (White) and averaged depth measurements(Black) . | 46 |
| 4.10 | Standardized (Solid) and approximate hardness results (Diagonal stripes). . | 48 |
| 4.11 | Resolution uncertainty histogram. | 49 |
| 4.12 | Load-displacement regression for tests on PC. | 55 |
| 4.13 | Load-displacement regression for tests on PC/ABS 80:20. | 55 |
| 4.14 | Load-displacement regression for tests on PC/ABS 70:30. | 56 |
| 4.15 | Load-displacement regression for tests on ABS. | 56 |
| 4.16 | Load vs regression residuals (Green: CU_{load} , Red: $rmse$ and Blue: Envelope). | 58 |

LIST OF TABLES

| | | |
|------|---|----|
| 3.1 | MTS Landmark calibration results. | 21 |
| 3.2 | Load transducer specifications [48]. | 21 |
| 3.3 | Mechanical properties of the R3 offshore grade steel. | 22 |
| 3.4 | LEXT OLS4100 accuracy values [50]. | 23 |
| 3.5 | Mechanical properties of the polymeric materials. | 23 |
| 4.1 | Hertz solution results at yield. | 39 |
| 4.2 | Maximum and minimum values of indicators for the data treatment. | 40 |
| 4.3 | Average standardized hardness of the specimens. | 47 |
| 4.4 | Load transducer combined uncertainty and components. | 49 |
| 4.5 | Static testing machine combined uncertainty and components. | 49 |
| 4.6 | Load combined uncertainties and components. | 50 |
| 4.7 | Average indentation diameters, standard deviation and expanded uncertainty. | 50 |
| 4.8 | Indentation diameter combined uncertainty and components. | 51 |
| 4.9 | Combined confocal uncertainty and components for indentation diameter. | 52 |
| 4.10 | Average indentation depth, standard deviation and expanded uncertainty. | 52 |
| 4.11 | Indentation depth combined uncertainty and components. | 53 |
| 4.12 | Combined confocal uncertainty and components for indentation depth. | 54 |
| 4.13 | Regression outputs and envelope key values. | 57 |

LIST OF SYMBOLS

| | |
|-------------------------------------|---------------------------------------|
| a | Half-length of the contact arch. |
| R | Indenter Radius. |
| $\delta, \delta_1, \delta_2$ | displacement. |
| P | Axial force. |
| S_1, S_2 | Surface. |
| T_1, T_2 | Body. |
| z, z_1, z_2 | Position along Z axis. |
| \bar{u}_1, \bar{u}_2 | Surface displacement. |
| E | Young's modulus. |
| E^* | Reduced elastic modulus. |
| ν | Poisson's ratio. |
| p_0 | Maximum contact pressure. |
| p | Contact pressure. |
| σ_y | Yield strength. |
| σ | Normal stress. |
| $\sigma_r, \sigma_\theta, \sigma_z$ | Normal stresses in polar coordinates. |

| | |
|--------------------------------|--|
| $\sigma_1, \sigma_2, \sigma_3$ | Principal stresses. |
| T_g | Glass transition temperature. |
| σ_p | Plastic flow stress. |
| ISE | Indentation size effects. |
| D | Indenter diameter. |
| d | Indentation diameter. |
| h | Indentation depth. |
| FS | Load transducer full scale. |
| HV | Vickers hardness. |
| HB | Brinell hardness. |
| U_i | Uncertainty contributor. |
| RSS | Root sum of squares. |
| CU | Combined uncertainty. |
| k | Coverage factor. |
| EU | Expanded uncertainty. |
| s | standard deviation. |
| n | number of occurrences. |
| U_{std} | Standard uncertainty of the mean. |
| U_{hys} | Hysteresis uncertainty. |
| U_r | Load transducer repeatability uncertainty. |
| U_{nl} | Non-linearity uncertainty. |

| | |
|-------------|--|
| CU_{lt} | Load transducer combined uncertainty. |
| F_i | Indicated force. |
| \bar{F} | Average indicated force. |
| F_n | Nominal force. |
| u_{rep} | Percentage repeatability uncertainty. |
| U_{rep} | Repeatability uncertainty. |
| U_{ue} | Uncorrected error uncertainty. |
| CU_{stm} | Static testing machine combined uncertainty. |
| N_{rg} | Noise range. |
| N_{avg} | Noise average. |
| U_{res} | Resolution uncertainty. |
| CU_{load} | Load combined uncertainty. |
| EU_{load} | Load expanded uncertainty. |
| U_{mean} | Uncertainty propagation in the mean. |
| u_{mt} | Percentage measurement tool uncertainty. |
| U_{mt} | Measurement tool uncertainty. |
| U_{acc} | Accuracy uncertainty. |
| CU_{con} | Confocal combined uncertainty. |
| CU_{dim} | Indentation mark dimension combined uncertainty. |
| EU_{dim} | Indentation mark dimension expanded uncertainty. |

| | |
|--------|--------------------------------|
| CU_h | Depth combined uncertainty. |
| EU_h | Depth expanded uncertainty. |
| CU_d | Diameter combined uncertainty. |
| EU_d | Diameter expanded uncertainty. |
| $rmse$ | Root-mean-square error. |

RESUMO

O processo de caracterização de materiais é composto por diversos procedimentos experimentais, como ensaios de dureza, tração e compressão. Esses ensaios requerem sistemas de teste e equipamentos de medição que geralmente contêm múltiplas fontes de incerteza. Por exemplo, ao realizar um teste de indentação em um sistema servo-hidráulico, o comando força axial está sujeito ao erro do transdutor de força, enquanto o sensor de deslocamento pode ser afetado por distúrbios no fluxo do fluido hidráulico. Além disso, o tipo de contato entre as amostras, seu posicionamento correto e sua qualidade geral de fabricação também podem exercer um papel significativo na precisão dos resultados. Portanto, tais incertezas contribuem para a dispersão geral das variáveis de interesse, nesse caso, profundidade e diâmetro da impressão de indentação.

O objetivo principal deste estudo é avaliar a influência das diversas fontes de incertezas presentes em um sistema de ensaio servo-hidráulico. Em particular, o foco da análise é dado à amostras poliméricas de Policarbonato (PC), Acrilonitrila-Butadieno-Estireno (ABS), uma mistura PC/ABS 70:30 e uma mistura PC/ABS 80:20. Os ensaios de indentação esfera-plano são realizados em uma MTS Landmark® e um novo dispositivo de acomodação de amostras. Os testes são realizados no regime elástico e após o surgimento de deformações inelásticas. As impressões de indentação são mensuradas com um microscópio confocal a laser.

Quatro níveis de carregamento são aplicados aos materiais testados: 500N, 1000N, 1500N e 2000N. A incerteza foi estudada para três variáveis de interesse: i) erro da força; ii) erro de medição do diâmetro da impressão de indentação; iii) erro de medição da profundidade da impressão de indentação.

As curvas força-deslocamento obtidas foram consistentes para todos os testes em PC e PC/ABS 70:30, inconsistentes para todas as configurações de PC/ABS 80:20 e para ABS em 500N e 1000N, e comprometidas para ensaios de ABS em 1500N e 2000N.

Ao todo, dez contribuintes de incerteza diferentes foram quantificados. As principais fontes de incerteza foram o transdutor de força, o microscópio e as medições da marca de indentação. Com base nos resultados da análise de incerteza, o equipamento se mostrou capaz de realizar testes de indentação de materiais poliméricos. Recomendações, baseadas nos resultados experimentais e nas observações feitas durante a análise, são fornecidas. Elas estão focadas no indentador, dispositivo de acomodação de amostras, procedimentos experimentais e amostras.

ABSTRACT

The process of material characterization is composed of various testing procedures such as hardness, tensile and compression analyzes. These tests require testing systems and measurement equipment which often contain multiple sources of uncertainty. For instance, when conducting an indentation test in a servo-hydraulic system, the axial force input is bound to the error of the loading transducer while the displacement sensor might be affected by disturbances in the flow of the hydraulic fluid. Moreover, the type of the contact between the testing samples, their correct placement and their overall quality of manufacture also can play a significant role in the accuracy of the results. Therefore, such uncertainties contribute to the overall dispersion of the variables of interest, in this case, depth and diameter of the indentation mark.

The main objective of this study is to assess the influence of the many sources of uncertainties present in a servo-hydraulic testing system. In particular, focus is given to the analysis of polymer samples of Polycarbonate (PC), Acrylonitrile-Butadiene-Styrene (ABS), a 70:30 PC/ABS blend and a 80:20 PC/ABS blend. Sphere-to-flat indentation tests are performed in a MTS Landmark® and a novel sample holder device. Tests are carried-out in the elastic regime and after the onset of inelastic strains. The indentation marks are measured with a confocal laser microscope.

Four load levels are applied to the materials tested: 500N, 1000N, 1500N and 2000N. The uncertainty was studied for three variables of interest: i) error of the load; ii) error of the measured diameter of the indentation mark; iii) error of the measured depth of the indentation mark.

The obtained load-displacement curves were consistent for all tests on PC and PC/ABS 70:30, inconsistent for all configurations of PC/ABS 80:20 and for ABS at 500N and 1000N and compromised for ABS tests at 1500N and 2000N.

Altogether, ten different uncertainty contributors were quantified. The major uncertainty sources were the load transducer, the microscope and the indentation marks measurements. Based on the uncertainty analysis results the equipment proved capable to perform indentation tests of polymeric materials. Recommendations, based on the observations made during analysis and from the test results, are provided. They are focused on the indenter, sample holder device, test procedure and specimens.

Chapter 1

INTRODUCTION

This chapter is structured in four sections which presents, respectively, a brief contextualization of the background and motivation related to the current study, as well as the research goals and a preview of the following chapters.

1.1 BACKGROUND AND MOTIVATION

Modern society is very familiar with plastics and the devastating COVID-19 pandemic accentuated the consumption of single-use items as a safety measure, reinforcing the relevance of this industry. Plastics are known for its low cost, lightweight, decorative looks and vast applicability, being valuable for different industries, like single-use items, household, automotive, construction, medical technologies, electronics, products and packaging.

There are several relevant chemical companies that, among other activities, develop and supply plastics worldwide, like BASF®, INEOS®, Ravago® and SABIC®. Among the materials used there is not only polymers, like PC and ABS, but also blends.

From the several companies developing and manufacturing plastic components, a Portuguese company called CODEPLAS® is related to this study. Their products, exemplified in Fig. 1.1, are destined for several industries, which in some cases requires not only good appearance, but also resistance to deformations, abrasion and wear.

Not only the suppliers, but also the companies using these materials, relies on properties, whether they are physical, electrical, thermal, optical or mechanical. These properties serves several purposes like design, processing, specification, quality control, failure analysis and development of new materials.

Properties are obtained through tests, that are developed to replicate specific states in which the desired properties are most relevant. This is achieved through procedures applied with scientific methodology, providing reliable and comparable results. Polymers testing is essential because of the rapid change within the plastics industry, allowing new material



(a) Gas cylinder components.



(b) Vehicles front grilles.



(c) Coffee maker parts.



(d) Electronics enclosures.

Figure 1.1: Polymer products manufactured by CODEPLAS®, extracted from [1].

developments, continuous refinements in manufacturing procedures and the discovery of innovative applications.

The present study is inserted in this context, in which two groups are testing polymer samples manufactured by CODEPLAS®. The first group, from the University of Porto, is carrying out conventional compression tests. The second group is from the University of Brasília and dedicated to test the material in conditions of wear and high inelastic deformation, several studies were accomplished [2–4] and many more are in development.

One of the projects developed intended to increase the testing capability of our laboratory, without the acquisition of new testing machines. The design of a novel device for indentation and fretting wear tests of solids with Hertzian geometry [5], developed as the final project of my undergraduate program, made to properly accommodate prismatic samples, to be tested with indenters presenting hemispherical or cylindrical tips, withstanding compression loads up to 10kN using MTS testing machines.

The lack of standard methods related to indentation and wear tests on polymers were a initial barrier, as well the necessary development of specific equipment and methods. These components are crucial to obtain meaningful and reliable results.

Since every test and measurement performed contains a certain level of uncertainty, the

current work was developed to assess the influence of uncertainty sources present in a servo-hydraulic testing system. Particularly focusing in sphere-to-flat indentation tests of polymer samples, performed in a MTS Landmark® using the novel sample holder.

1.2 RESEARCH GOALS

This work is mainly focused at the analysis of uncertainties present in a servo-hydraulic testing system during sphere-to-flat indentation tests of polymer samples, to verify the suitability of the equipment available for polymer testing and analysis. A secondary goal is to carry out a qualitative analysis of the entire experimental process, achieving not only the guidelines for an ideal experimental methodology and the post test analysis.

Towards these goals, several distinct tasks are defined scaling to fulfill the general purpose:

- Identify sources of uncertainty;
- Verify the impact of using materials from different suppliers;
- Check the suitability of chosen load levels for the provided samples;
- Identify main uncertainty contributors for load, indentation and diameter and depth;
- Obtain the average behavior of the four materials in study with uncertainty envelope;
- Point out means for improvements and corrections of the applied methodology.

1.3 OUTLINE

This work is structured in five chapters as follows:

Chapter 2 presents a literature overview regarding the most relevant concepts related to this study. It is divided in four sections:

- Polymers: starting at a brief historical background of polymer development, then both studied materials are briefly discussed, including their applications and characteristics. At last polymer blending is introduced and the specifics of the blend used in this study is presented.
- Contact Mechanics: this section is divided in two subsections, the first one presents a comprehensive review of the well known Hertz Theory of Elastic Contact, focused at the sphere-to-flat solution. Describing the contact geometry, equations for the analytical solution and the identification of the onset of plastic yield. The second subsection

contains a brief description of the viscoelastic behavior, focusing on the source of non-linearity.

- Compression tests: presents the major aspects of the compression tests, relation and outline of indentation tests, application of indentation to obtain hardness including a discussion over the size-scale effect and the related standardized procedures for all mentioned tests.
- Multi-uncertainty: contains the definition of uncertainty along with the reason to quantify it, the most common sources for mechanical testing in general, specific sources for indentation tests.

The materials and methods employed to accomplish the goals of this study are thoroughly presented in Chapter 3. It also approaches the uncertainty analysis developed as well as the data treatment necessary to overcome issues identified in the collected data.

Chapter 4 contains all results gathered and calculated. During their presentation discussions are made based on the observations.

Chapter 5 presents a summary of the most relevant discussions made in the preceding chapters along with the recommendations for future studies to improve results and address specific events observed during the current study.

Chapter 2

CONCEPTS

In this chapter an overview of the most relevant concepts for the present study are given. Firstly the historical background of polymers in general is presented including characteristics, classification and applications. Then, details related to the polymers and blends used in this study are provided.

The second part is a description of concepts related to contact mechanics, including the Hertzian formulae and the nonlinear behavior of solids in contact. Lastly a brief introduction to multi-uncertainty and examples of uncertainty sources in indentation tests is presented.

2.1 POLYMERS

First documents describing its use go back to the age of navigations when reports from Christopher Columbus describe the Haiti natives playing with balls made out of material obtained from a tree. This material is an organic emulsion named as latex, also known as natural rubber (NR) [6].

The synthetic polymers industry dates from the 19th century with modifications of shellac, natural rubber, gutta-percha (GP) and cellulose. The first polymer blend, NR with GP was patented in 1864 with applications ranging from picture frames to sheathing the first submarine cables [7].

Since its beginning this industry evolved through the understanding of molecular structure, material properties and how they could be modified and combined in order to achieve desired characteristics. In early 1900s there was a rapid commercial development of many important synthetic polymers, usually referred as plastics, and it followed an even faster pace after the war. The world production in 1900 was about 30,000ton [7] and according to the Plastics Europe Research Group, 359 million tons were produced in 2018. In Europe the three major segments for that same year were Packaging with 39.9%, Building & Construction with 19.8% and Automotive with 9.9% [8]. Among several contributions in this period Acrylonitrile-butadiene-styrene (ABS) was developed in 1948 and Polycarbonate (PC) also

dates from the 1950s [9].

Plastics materials are popular for many different reasons, like transparency, self-lubrication, lightweight, flexibility, low cost and decorative looks. These properties can be modified using fillers, reinforcing agents and chemical additives. These processes benefits many engineering applications, such as mechanical components under stress, low-friction surfaces, heat and chemical resistant units, electrical parts, housing, building construction functions, and many others [9].

There are several polymer classification methods, such as: by its nature, as Natural or Synthetic, based on its molecular composition as addition polymers or condensation polymers, and finally due the application field, as commodity, engineering and specialty. Addition polymers have their main chains consisting entirely of C-C bond whereas Condensation polymers presents hetero atoms (e.g., O, N, S, Si) in the polymer backbone. Commodity polymers are those produced in high volumes for applications where exceptional properties are not needed, they tend to be inexpensive, while engineering polymers presents better mechanical properties and are more expensive [9].

In the following, the synthetic polymers employed for this study are introduced. Organized in three sections, some aspects regarding PC, ABS and PC/ABS blends are presented including compositions, general characteristics, manufacturing and applications.

2.1.1 POLYCARBONATE (PC)

Polycarbonates are formed by two monomers: Bisphenol A and phosgene. Although it is generally processed trough injection molding or extrusion, all thermoplastic-molding methods can be applied. Material presents limited chemical resistance, high impact strength, transparency, great electrical insulation, toughness and heat and flame resistance [9].

It is adequate for many applications but its extensively used in electronics and electrical engineering being used as cover for time switches, batteries, and relays, coil formers, computer and calculating machines, magnetic disk pack housing and starter enclosures for fluorescent lamps. Since its ability to stand all sterilization methods there are traditional applications in the medical market as filter housings, tubing connectors and surgical staplers. There was also a continuing growth of the market for polycarbonate glazing and light transmission units [9].

2.1.2 ACRYLONITRILE-BUTADINE-STYRENE (ABS)

ABS polymers, as the name suggests, are formed by three different monomers: acrylonitrile, butadine and styrene that are generally presented at the following respective ratios: 20-30%, 20-30% and 40-60% [10]. Each monomer contributes with distinct properties. Acrylonitrile provides chemical and heat resistance and high strength; butadiene contributes

toughness, impact strength and low-temperature property retention; styrene brings rigidity, surface appearance and processability. Both monomers ratio and assembly can be varied, giving ABS a very large range of material types [9].

They can be processed by all common techniques used with thermoplastics and machining characteristics are similar to those of nonferrous metals. Its light weight, adequate chemical resistance and with very good surface finish achieved on molded specimens aligned with its costs have contributed to several applications such as household items, telephone handsets, electrical hand tools, handles, knobs, bearings, wheels, gears, sporting goods, consumer electronics, among many others. The major uses are for Pipe and fittings, automotive and appliance, telephones and business machines housings [9].

2.1.3 PC/ABS BLENDS

Simply stating, polymer blends are mixtures of two or more polymers with no chemical interaction between them. Due to the difficulty and amount of time necessary in developing new polymeric materials from monomers there was a considerable interest in blending, since it can be more cost-effective to combine usually two known polymers to achieve desired properties [10, 11].

To major resin manufacturer, blending is a mean to improve and broaden the resin performance, enhancing demands and sale, while users starts with a set of properties that the material must posses. In both cases to achieve desired characteristics a component that already shows this characteristic must be used [7].

This process can result in miscible or immiscible polyblends, resulting in separate phases since most polymers are not miscible. Miscibility is not a prerequisite to commercial utility though its more convenient from the standpoint of properties prediction and processing characteristics. The optimum requirements for completely miscible polymers are similar polarity, low molecular weight and a strong intermolecular attraction. In this case it would be expected properties following a simple monotonic function, sort of proportional to the contents [9].

The immiscibility level can vary, affecting blend properties. Slightly immiscible components results in phases of solid solution of the minor polymer in major polymer, separated in submicroscopic domains with a continuous matrix phase of the major polymer, which contributes the most toward final properties. Most commercial blends are of this type. For more immiscible components the blend presents a phase separation of larger domains with weaker interfacial bonding, which are more susceptible to fail under stress and final properties are thus likely to be poorer than either of the used polymers [9].

By combining the good processability of ABS with mechanical properties, impact and heat resistance of PC its possible to achieve a immiscible, two-phased, material with dimensional stability, low shrinkage and moisture absorption, high stiffness and hardness, good

impact resistance in low temperatures, processability, mechanical properties, flame retardant and heat resistance. Blends are obtained with either a co-continuous or dispersed morphology [7].

Some papers concerning blends properties were delivered but results concerning PC/ABS blends are unclear and sometimes contradictory. This can be explained by a third component present (butadiene-acrylonitrile copolymer) resulting in these three distinct phase interacting. There is also a great number of variables influencing properties and morphology such as PC and ABS molecular characteristics, ABS internal composition, mixing techniques and final processing [12]. Moreover, studies regarding the performance of PC/ABS blends in contact applications are rather scarce.

2.2 CONTACT MECHANICS

Contact mechanics is a field of study that addresses relative motion, deformation and stresses originated due to contacting solids. From the engineering perspective this principles can be implemented towards applications like bearings, transmission line cables, chain links, combustion engines, contact welding, sealing and braking systems. As most known mechanical properties of materials those relating to contact also depends on several factors.

Another popular application is through indentation, where properties like elastic modulus and hardness can be extracted. In this process an impression is generated on the specimen surface by a tool, desired information are obtained based on the mark dimensions and the applied loading. The tool used is called indenter, they are made out of a material with hardness values higher than the material in study. There are several geometries used but most common are either pyramidal or spherical, which is the scope of this work and will be addressed in details.

2.2.1 SPHERE-TO-FLAT HERTZIAN SOLUTION

Among the studies developed by Hertz there is a theory developed regarding the normal contact of elastic solids. The contact of two non-conforming solids starts at a single point or along a line. Deformation due to the applied load happens in the vicinity creating the contact area between the solids and this theory allows the prediction of the contact area growth along with the pressure, deformation and stress in both solids at their contact region.

During the formulation of this theory, Hertz introduced some simplifications. The first one is that the contact area is, in general, elliptical. In order to calculate the local deformations each body was regarded as an elastic half-space, by doing this the highly concentrated stresses are separated from the general distribution of stress on both bodies, that arises from their shape and support. To justify this simplification the contact area must be small compared with the body dimensions and the relative radii of curvature of the surfaces. The aim

of the first consideration is ensuring that the stress field is not seriously influenced by its boundaries, and the second ensures that the strains in the contact region lies within the elastic theory. The last simplification is the absence of friction, thus only a normal pressure is transmitted [13].

This assumptions may be summarized as follows:

- The surfaces are continuous and non conforming (implying that the area of contact is much smaller than the characteristic dimensions of the contacting bodies): $a \ll R$;
- The strains are small and within the elastic limit: $a \ll R$;
- Each body can be considered an elastic half space: $a \ll R_{1,2}, a \ll l$;
- The surfaces are frictionless: $q_x = q_y = 0$.

At first the geometry of the solids in contact is carried out in a Cartesian plane. The contacting surfaces expressions are described, as well as the separation between them and using a geometry relations an equivalent radius, R_e , is defined.

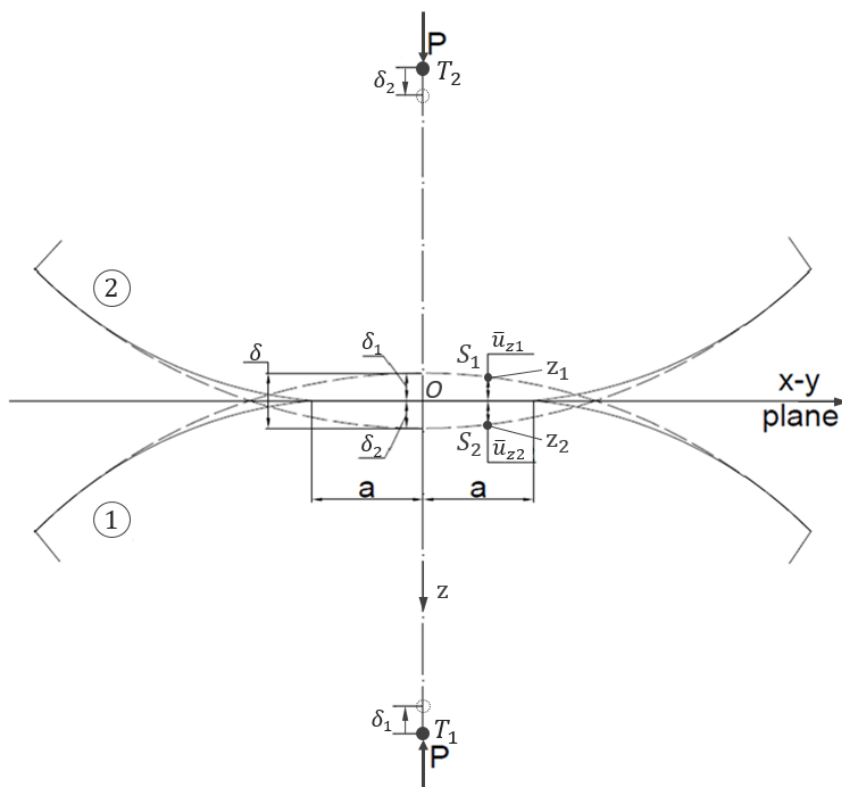


Figure 2.1: Contact geometry of non-conforming solids under normal compressive load [13].

Figure 2.1 shows that under a normal compressive load, P , the initial contact point is defined, the separation between two corresponding surface points $S_1(x, y, z_1)$ and $S_2(x, y, z_2)$ is given by the subtraction of the z component. A movement parallel to the z -axis is achieved during compression and the distant points of the bodies T_1 and T_2 move towards O by δ_1 and

δ_2 , resulting in a total displacement $\delta = \delta_1 + \delta_2$. If there was no deformation of the solids their profiles would overlap as the dotted lines, but as mentioned beforehand the point of contact spreads into an area and each surface displaces by \bar{u}_{z1} and \bar{u}_{z2} due to the contact pressure, making points S_1 and S_2 coincident within the contact surface, the boundary condition for displacements within the contact zone may be expressed as:

$$\bar{u}_{z1} + \bar{u}_{z2} = \delta - (1/2R)r^2 \quad (2.1)$$

Elasticity is then introduced relating the estimated deformation with the contact pressure divided by the elastic modulus. This allows a relation between the applied force and the compression with the local indentations. The expression regarding the equivalent radius of contacting spheres is $(1/R) = (1/R_1 + 1/R_2)$ and the obtained equations for contact area radius, total displacement, maximum contact pressure and pressure distribution along contact radius are presented below. These equations can be applied for sphere-to-flat contact considering the plane a sphere with infinite radius.

$$\begin{cases} \frac{1}{E^*} = \frac{1-\nu_1^2}{E_1} + \frac{1-\nu_2^2}{E_2} \\ a = \left(\frac{3PR}{4E^*}\right)^{(1/3)} \\ \delta = \frac{a^2}{R} = \left(\frac{9P^2}{16RE^{*2}}\right)^{(1/3)} \\ p_0 = \frac{3P}{2\pi a^2} = \left(\frac{6PE^{*2}}{\pi^3 R^2}\right)^{(1/3)} \\ p = p_0\{1 - (r/a)^2\}^{1/2} \end{cases} \quad (2.2)$$

Onset of plastic yield of most ductile materials is usually taken to be governed by von Mises shear strain-energy criterion, given by Eq. (2.3) in function of the principal stresses.

$$\frac{1}{6}\{(\sigma_1 - \sigma_2)^2 + (\sigma_2 - \sigma_3)^2 + (\sigma_3 - \sigma_1)^2\} = \frac{\sigma_y^2}{2} \quad (2.3)$$

For the axi-symmetric contact of solids of revolution the maximum shear stress in the contact stress field occurs beneath the surface over the axis of symmetry, where σ_z , σ_r and σ_θ are the principal stresses and $\sigma_r = \sigma_\theta$. Considering a ring of concentrate force at radius r , stresses are calculated using the following equations:

$$\frac{\sigma_r}{p_0} = \frac{\sigma_\theta}{p_0} = -(1 + \nu) \left\{ 1 - \left(\frac{z}{a}\right) \tan^{-1} \left(\frac{a}{z}\right) \right\} + \frac{1}{2} \left(1 + \frac{z^2}{a^2} \right)^{-1} \quad (2.4)$$

$$\frac{\sigma_z}{p_0} = - \left(1 + \frac{z^2}{a^2} \right)^{-1} \quad (2.5)$$

where ν is the Poisson's ratio and z is the position along Z axis.

2.2.2 NON-LINEAR MATERIAL BEHAVIOR

Elastic-plastic materials such as metals presents a well known behavior that consists of two regimes, the yield strength is the stress value that defines the point of transition. Stresses below it cause only elastic deformations, which are the primary type and disappear once loading is removed. Once that critical value is exceeded a second component of the deformation caused and it is permanent, known as plastic deformation. Both processes, the appearance of both components during loading, and the regeneration of the elastic during unloading, are usually assumed as instantaneous [14].

The beginning of the plastic flow, and subsequent events, relies at the classic macroscopic approach of the problem, using semi-empirical yield criterion like Tresca and von Mises. This is a consequence of assuming that strain measures are linear, neglecting the non-linear aspect of the transition region, creep and relaxation [15].

When most simple compounds like metals are cooled below their melting temperature they crystallize, but for more complex materials such as polymers this process might not happen. During this process the viscosity can rapidly increase as temperature is reduced, preventing partially or completely the intermolecular arrangement. Once a critical temperature is achieved and the material turns into glass, ergo it is known as the glass transition temperature, T_g , [16, 17].

Mechanical and physical properties of a material are directly related to the type of bonding between its molecules, and thermoplastic polymers tend to present weaker secondary bonds between their long molecule chains. In most cases the molecules are randomly arranged, these polymers are classified as amorphous. Other polymers consists of chains arranged in a structured manner, exhibiting limited crystallinity [17, 18].

The characteristics mentioned introduces rheological phenomena to the behavior of polymers, and among them is the viscoelasticity. A third type deformation is introduced, originated from the distortion of the polymer chains from their equilibrium conformation, which is reversible over time [19].

If the distortion applied is relatively small it can be easily removed by heating the sample to just above T_g , thus taking the material to the glass transition region, which increases the molecular motion promoting structural relaxation. Even when the deformation greatly surpass the yield point, real glassy polymers still tends to get back to its original structure. There are also other types of relaxations referred as secondaries, they happen at temperatures below T_g and are belived to promote much more localized motions [20, 21].

The conventional stress-strain curve of glassy polymers obtained by a tensile test is shown in Fig. 2.2. The curve can be separated in four distinct zones:

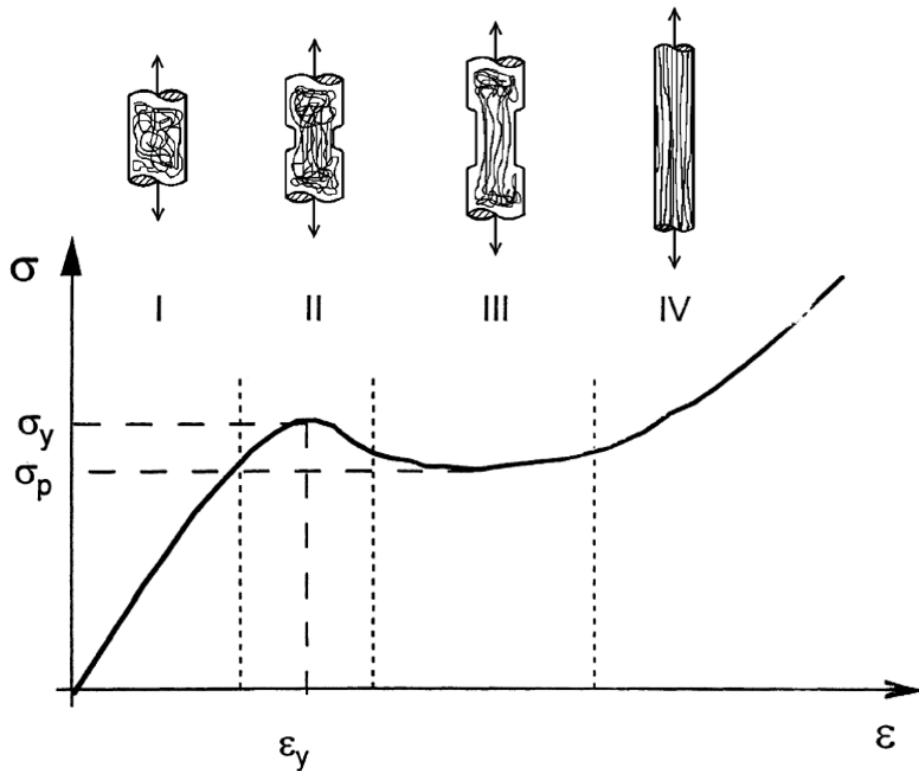


Figure 2.2: Representation of stress-strain curve of a glassy polymer, adapted from [22, 23].

- Elastic Regime: presence of secondary relaxations but with low impact, therefore, the material presents a nearly linear behavior. This zone ends once the viscoelastic response promotes significant change in behavior [21];
- Transition Zone: relaxation response increases causing the decrease of the slope, stress increases up to σ_y , then inelastic deformation is developed and the neck evolves as the stress drops, exhibiting strain softening [21];
- Steady State Regime: the neck becomes stable at the minimum value, called plastic flow stress, σ_p . Crazes are cracks containing fibrils able to sustain stress, dissipating energy during propagation. This mechanism allows deformation to proceed with small stress variation, representing a creep response of the material at the neck, as the fibrils creep [24, 25];
- Strain Hardening: The deformation reaches a point where the mobility of the chains are reduced enough and the stress begins to increase again. At last, the strain hardening relevance gradually increases along with the crazes until the material fails [24, 25].

During uniaxial compression, the material behavior is similar to results obtained from tensile tests. Crazes are developed only under tension while shear yielding is the failure mode acting under compression conditions. It causes the local transverse area to increase, reducing the local true stress which stabilizes the region being deformed, causing the same post-yield strain softening [25, 26].

Since the deformation is applied over the same axis, but in the opposite direction, the chain segments tend to be arranged in the transverse direction and away from the direction of the loading. The effect is the development of an induced anisotropy due to the deformation, which implies in a higher strain value. This indicates that the hardening occurs much later, and since the stress-strain presents the same behavior, the yield stress will also be higher during compression [22, 24, 26].

2.3 COMPRESSION TESTS

This study primarily encompasses two fields of research: i) mechanical characterization of solids using compression tests; and ii) surface hardness measurement via indentation tests. Relevant references related to these topics are provided in the following, including standardized test methods.

Data obtained from compression tests provides a precise comprehension of the material behavior under this specific loading condition, being complementary to tensile test results since not all material shows tension-compression symmetry.

The test consists of the compression of a specimen, usually cylindrical, by flat and parallel bearing blocks, as shown in Fig. 2.3. Once the specimen is properly aligned between the blocks, or flat plates, a displacement is applied to one end at a controlled speed, which provides the strain-rate, until failure or past yield strength depending on the material behavior.

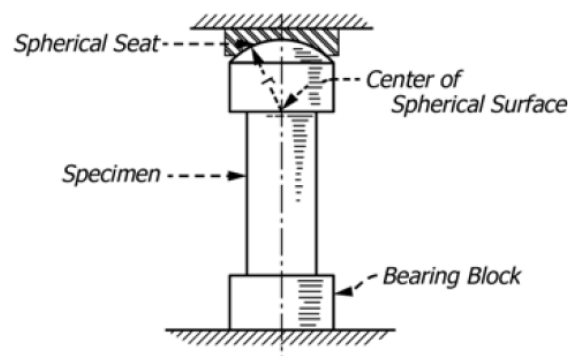


Figure 2.3: Compression test with a spherical-seated bearing block [27].

Differently from tensile tests, necking does not occur under compression, but other complications like buckling and barreling might complicate results and should be minimized. Results obtained, which are only comparable to specimens produced and tested under exactly same conditions, might include: yield strength, compressive modulus, stress-strain curve, compressive strength and nominal strains at yield and break [28].

2.3.1 INDENTATION TESTS

Differently from compression tests, which a hole specimen is compressed, the indentation process is a variation that consists in the application of a specified compressive load to the specimen surface through a tool known as indenter, that might present different geometries [29].

The mechanism behind the indentation process is versatile and essential to contact mechanics in general, seen in classical theories as the hertzian solution and concepts that emerges from it, but also in more complex states like fretting wear and abrasion.

Besides the simplicity of the equations presented in the Hertzian solution, the mechanism involves complex stress and strain fields. Not only the material behavior also affects the process, considering elastoplasticity and the presence of viscous phenomena, but also the size scale of the indentation.

Since the popularization of this kind of tests, indentation size effects (ISE) were observed as they were minimized. At first ISE were somewhat unclear, due to uncertainties of measurements and poor geometry of the indenters. With the advance of technology, above all in instrumentation, these sources of errors were greatly removed and the real physical basis were put in evidence [30, 31].

An expression became popular: "smaller is stronger". The ISE is related with the material morphology and the induced plastic flow of the material at the contact zone surroundings. As the size scale goes from macro to micro and nano, the deformed volume decreases limiting the dislocations, leading to increased strength. It is reported that for conical and pyramidal indenters there is a dependence of the measured properties with the indentation depth, while for spherical indenters it relates to the diameter of the indenter [30, 32, 33].

The most common application is hardness testing, used to probe the mechanical behavior of materials, being well known and presenting some standardized test methods. It is mostly used for being a simple, easy and relatively nondestructive way of property evaluation that requires minimal specimen preparation and mounting [29, 34].

2.3.2 HARDNESS TESTS

Hardness is interpreted as superficial resistance to permanent indentation and even though it is not a fundamental property of a material, it might present relationship with other mechanical properties. The main purpose of this test is to provide information on the suitability of a material for a given application, or treatment to which it has been subjected [29].

Hardness value usually arise from the impression dimensions and it only has quantitative value in terms of the specific configuration composed by: load, duration and indenter shape. This method to obtain the hardness value is controlled by a plastic property of the material being tested. Instrumented indentation provides an alternative method which the

hardness value and other elasto-plastic properties are extracted using the load-displacement curve, or contact compliance curve, captured during both loading and unloading stages [35].

Specifically on thermoplastic materials, they present very complex deformation properties, both the elastic modulus (E) and yield strength (σ_y) depends on the deformation rate. For most of them the ratio of E/σ_y is of order 10, significantly lower than the 100-1000 value for metals, this indicates that there is less plastic flow constraints and the expected hardness values are also lower [30].

2.3.3 STANDARDIZED TESTS

Standards generates a reliable and reproducible method for obtaining data, it specifies different aspects like test scope, referenced documents, terminology, significance and use, apparatus, test specimen definitions, procedure description, conditioning, calibration, precision and bias in addition to report format [36]. In the following, four different standard procedures are presented, two regarding compression tests and two regarding hardness tests..

- ASTM E9-19 - Standard test methods of compression testing of metallic materials at room temperature

The standard ASTM E9-19 [27] describes the test methods of compression testing of metallic materials at room temperature. In order to assure the suitability of the test apparatus, a preliminary qualification test is necessary. This process consists of tests conducted in five specimens, with the smaller suggested dimensions, of 2024 T3 aluminum alloy in accordance with the test method provided. The qualification is achieved once the elastic modulus obtained for each specimen lies within $73.8GPa \pm 5\%$.

Three different forms are suggested for cylindrical test specimens, designated as short, medium and large, with the dimensions and deviations as specified. Thin-sheet specimens might also be used, as long as they are flat, with the full thickness of the material and with sufficient length that allows the specimen to shorten the amount required to define the desired properties without the presence of buckling. Surface roughness, flatness and parallelism shall also be in accordance to the respective specified values.

Once the specimen is measured, cleaned, lubricated and properly installed, the test is conducted at the prescribed rate. Brittle materials that fail by crushing or shattering may be tested to failure, while Ductile materials may have the test halted after yield strength can be determined. The compressive strength of ductile materials is a value that depends on total strain and the specimen geometry. Once the test is complete, properties are determined from the dimensions of the specimen and the stress-strain diagram, following the described calculations when necessary.

- ASTM D695-15 - Standard test method for compressive properties of rigid plastics

The standard test method for compressive properties of rigid plastics is defined by the ASTM D695-15 [37], specific standards addresses testing of resin-matrix composites. Once again an observation is made regarding the compressive strength, which is an arbitrary value, for materials that do not fail by a shattering fracture, that depends upon the degree of distortion characterizing complete failure of the material. Many polymers shows a perfectly plastic behavior with continuous deformation in compression until a flat disk is produced, the nominal stress rises steadily in the process, without a clear sign of fracture. In such cases the compressive strength do not have a real meaning.

The test machine and auxiliary equipment must also conform to indicated specifications, with no qualification test necessary for suitability evaluation. The compression tool must also be flat and parallel to properly apply the load to the test specimen. The specimen geometry shall be preferably cylindrical or prismatic, but alternative specimens are indicated including special cases for thinner materials.

Ambient conditions may affect the studied material, arising the need to provide correct storage and conditioning. The common sense is to avoid material exposure to degenerative influences such as high temperatures, humidity and UV light in addition to consider time interval between production and testing. The standard atmosphere description in ISO 291 [38] and ASTM D618 [39] is 23°C and 50% relative humidity (RH) but in tropical countries 27°C and 65% RH is allowed for all polymeric materials [40].

At least five specimens must be tested for isotropic materials and in presence of anisotropy five additional tests shall be conducted parallel to the principal axis. The testing procedure is similar to the one applied to metallic materials, with different test speed specifications, and all additional procedures necessary to obtain the desired properties are also presented.

- ASTM E10-00 - Standard test method for Brinell hardness of metallic materials

The standard test method for Brinell hardness of metallic materials, ASTM E10-00 [41], mentions loads up to 3000kgf using balls polished and free of surface defects, with diameter between 1-10mm and deviation smaller than $5\mu m$. There is no specification for the specimen thickness as long as no bulge or other marking showing the effect of the test force appears on the side opposite to the indentation, recommending a general rule of the thickness being at least ten times the indentation depth.

E 10-00 also indicates that the testing machine must not have an error in the test force greater than $\pm 1\%$, it is recommended that the diameter of the indentation be between 24-60% of the ball diameter and at least five indentations shall be made, respecting a distance of at least 2 and a half times the indentation diameter from the center of the indentation to the edge of the specimen or edge of another indentation.

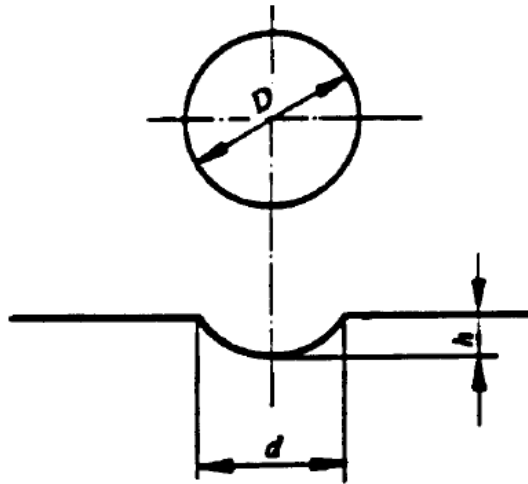


Figure 2.4: Principle of Brinell hardness tests [41].

The Brinell hardness number is given by the relation:

$$HB = 0.102 \times \frac{2F}{\pi D(D - \sqrt{D^2 - d^2})} \quad (2.6)$$

where D is the diameter of the sphere in mm, F is the test force in N and d is the mean diameter of the indentation in mm.

- ASTM D785-03 - Standard test method for Rockwell hardness of plastics

There is also a specified standard test method for Rockwell hardness of plastics, ASTM D785-03 [42]. It establishes major loads up to 150kgf using indenters with diameter between 3.175-12.7mm, the allowed deviation is ± 0.0025 mm and the tip must be free of nicks or burrs. It is recommended that the test specimen shall have a minimum thickness of 6mm and at be least 25mm squared with parallel flat surfaces. A note mentions that specimens with a thickness other than 6mm may be used if no imprint shows under the specimen after testing. Any bulge, change in color, or other marking on the under surface is an indication that the specimen is not sufficiently thick.

The same recommendation of at least five indentations is made, respecting a clearance of 6mm to the edge of the specimen, and in under no circumstances the opposite face of a tested specimen shall be used. Other relevant observations are that a large ball indenter tends to distribute the load more evenly, decreasing the range of test results; samples with a molded finish provides higher Rockwell readings than a machined face and the last one states that an anisotropic material generally shows higher readings at faces perpendicular to the molding pressure.

2.4 MULTI-UNCERTAINTY

Uncertainty might be defined as a parameter, associated to a measurement, that characterize the dispersion of the values imputed to the measurand or even an estimate of the range of values that includes the real value of the measurand [43].

Every test performed provides results with limitations and its a known fact that measurement variability occurs due to numerous sources. Spread of results arises from non-homogeneous samples, use of different batches, difference in ingredients or mixing process, manufacturing process variability, differences in test piece preparation, test procedures variability, machine calibration, operator error among other factors [36,40,44,45].

Specifically on hardness and indentation tests the most common errors are caused by: the zero error at the beginning of the test, uncorrected error of the test machine, the force transducer or deviation in the indenter geometry [46].

Almost every test relies in the measurement of at least one critical dimension to obtain the final result, the measuring process not only translates but also insert errors and uncertainties in the test results. An appropriate device must be selected, considering the type and scale of the measurement, so that additional factors can be minimized and correctly accounted for. Moreover, a propagation analysis of these contributions is also advised [36,40].

Regarding the measuring process, errors and uncertainties can arise from the following sources:

- measuring instrument,
- item being measured,
- measuring process,
- operator skill,
- sampling issues
- environment.

Although the words error and uncertainty are used in some situations as synonyms, they represent different concepts that have some similarities and in some cases might be related. Differently from uncertainty, error is the actual difference between the true and measured values. Corrections can be quantified and applied to measurements, usually defined in calibration certificates, but errors whose values are unknown becomes a source of uncertainty [44].

Besides sharing the same sources, both might be classified as random and systematic, depending respectively on the lack or presence of value consistency among repeated measurements. Its important to differentiate the contributions that directly impacts the measurement from material, manufacturing or methodology inconsistency [43,44].

Chapter 3

MATERIALS AND METHODS

As previously mentioned, this study is a follow-up to the design of the sample holder device. More specifically, it aims to evaluate the viability of the current test setup and methodology for indentation tests of polymer samples. All aspects from the sample preparation through post-test microscopic inspection were evaluated and an in-depth uncertainty analysis was carried out considering the equipment used in the process.

Performed activities can be divided into seven main groups: Analytical solution, Sample preparation, Hardness tests, Indentation tests, Microscopic inspection, Data treatment and Uncertainty Analysis.

This chapter is divided into four sections. Firstly are presented: the equipment employed, with their respective specifications, and sample properties along with the preparation process. The second section contains a description of all testing procedures, followed by the uncertainty analysis, which includes aspects of the manufacture errors, repeatability and measurement errors. Lastly the data treatment process is described in detail.

3.1 EXPERIMENTAL SETUP

All tested samples were prepared beforehand through grinding and polishing procedures then Vickers and Brinell Hardness tests were performed. The indentation test setup consisted of four components: testing machine, sample holder device, hemispherical tip indenter and specimen. All equipment and processes necessary are presented in the following sections, as well as material properties and relevant equipment specifications.

3.1.1 EQUIPMENT

This section aims to describe in detail the used machines and equipment in addition to specifications relevant to the study scope.

- Vernier Caliper

A Mitutoyo Vernier Caliper was used for thickness evaluation during the sample preparation process. The model used presents 0.05mm graduation with 0.02mm accuracy.

- Metallographic Grinding and Polishing Machine

Also during specimen preparation a PANTEC POLIPAN-U grinding and polishing machine was used with three purposes: thickness adjustment, surface grinding and polishing. The machine used was manual, single wheeled with variable speed and had interchangeable disks for each task. Different wet sandpaper disks were used with grits: 120, 240, 320, 400, 600, 800 and 1200.

- Micro-indentation System

Micro-Hardness tests were performed with the EMCO-TEST DuraScan 20 using a Vickers micro-indenter applying a 0.1N load (HV 0.1). This machine has an automatic test cycle, providing the measured hardness value through a digital display once the cycle is complete and indentation mark is measured through its software.

- Universal Hardness Tester

Brinell Hardness testes were conducted with the Zwick/Roell ZHU 250 Universal Hardness Machine using a tungsten carbide sphere indenter of 2.5mm diameter the 300N load was applied (HBW 2.5/300). This machine has an automatic test cycle, requiring manual measurements of the indentation impression using the coupled measurement tool, in order to provide hardness reading through its digital display.

- Axial Test Machine

The indentation tests were fulfilled with MTS Landmark®370 Servohydraulic Test System, an axial test machine with crosshead-mounted actuation, as Fig. 3.1 represents. Load readings are provided by a Force Transducer with 5kN capacity and linear actuator's displacement is measured by a Linear Variable Displacement Transducer (LVDT).

The 370.10 LVDT is located inside the actuators, with ± 100 mm capacity is located inside the actuators. The last calibration reports the Eq. (3.1) for measurement uncertainty, in mm, valid for the full range as function of the absolute displacement (IDI). The minimum uncertainty would be $52.0\mu m$, since the maximum test displacement was 3.4mm and measured indentation depth ranged between 1.33 - $142.33\mu m$, this uncertainty source was not taken into account.

$$U_{lvd} = \pm(0,052 + IDI/58425.1) \quad (3.1)$$

Last Landmark calibration was also performed for the load and the same transducer is equipped, Tab. 3.1 presents the obtained values of expanded uncertainty for each nominal load.



Figure 3.1: MTS Landmark@370 test machine with crosshead-mounted actuation [47].

Table 3.1: MTS Landmark calibration results.

| Load [N] | U95% [N] |
|--------------|----------|
| -500 | 1.26 |
| -1000 | 2.12 |
| -2000 | 3.15 |

- Load Transducer

The 661.19F-01 force transducer capture load readings during the experiment, directly affecting load accuracy and uncertainty. Table 3.2 shows three specifications and their respective values, which were considered as uncertainty sources: Non-linearity (U_{nl}), Hysteresis (U_{hys}) and Repeatability (U_r).

Table 3.2: Load transducer specifications [48].

| Model | Full Scale (FS) | Non-linearity | Hysteresis | Repeatability |
|------------|-----------------|---------------|------------|---------------|
| 661.19F-01 | 5 kN | 0.08 %FS | 0.05 %FS | 0.03 %FS |

- Sample Holder Device

The sample holder device, Fig. 3.2, was designed for sphere-to-flat compression tests. It can also be employed for fretting wear analysis, withstanding not only pure compression but also torsional moment [4]. Design process considered AISI 1020 steel for the device and hemispherical tip pad with 50mm radius, for tests on 2024-T3 Aluminum samples.

This configuration was capable to withstand compression loads up to 10kN while

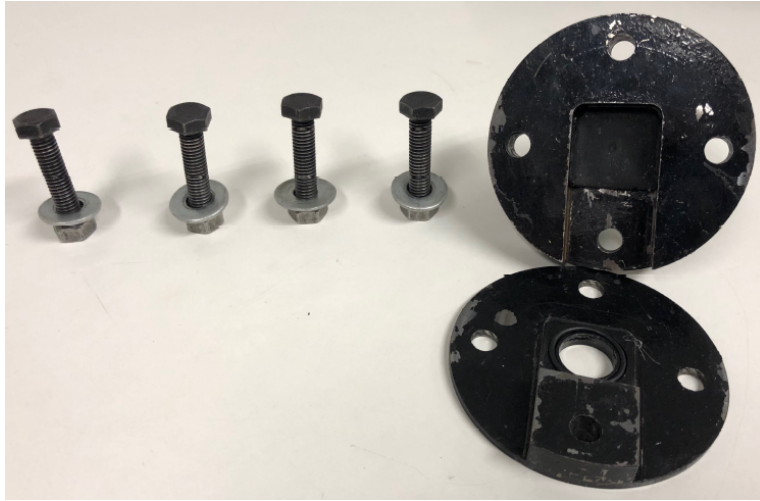


Figure 3.2: Sample holder device [3].

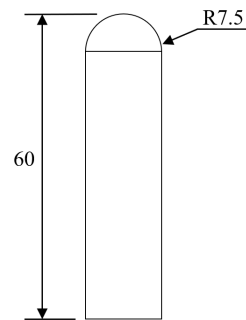
reaching a maximum von Mises equivalent stress equal to 260MPa, approximately half of the yielding limit of the steel used for the manufacture of this device. Adopted specimen geometry was prismatic, measuring 25mm x 25mm x 5mm, and rubber sheets were placed inside the slot for proper accommodation [5, 49].

- Hemispherical Tip Indenter

Figure 3.3a shows one of the indenters used in the experiments. They have 60mm in length and 7.5mm tip radius, as represented in Fig. 3.3b.



(a)



(b)

Figure 3.3: (a) Hemispherical tip indenter and (b) dimensions in mm .

They were CNC machined out of R3-graded offshore steel, with a final cutting pass applied to check radial uniformity, and the tip was sanded using a 2400 grit sandpaper. Table 3.3 presents the R3 steel mechanical properties.

Table 3.3: Mechanical properties of the R3 offshore grade steel.

| E [MPa] | σ_y [MPa] | ν |
|----------------|------------------------------------|-------------------------|
| 207000 | 410 | 0.34 |

- Cofocal Laser Microscope

The microscopic inspection of the indentation marks were executed with a OLYMPUS LEXT OLS4100 confocal laser microscope. This device scans the sample, in both laser and color spectrum. The inspection generated 3D models of the indentation marks and its periphery.

The software provided with the microscope have a measurement environment that allows the user to control the displayed 2D profile of the generated model cross-section, and posses tools to obtain desired dimensions. Table 3.4 presents accuracy and a 5% error was adopted for the measurement tool, both were considered as uncertainty contributors.

Table 3.4: LEXT OLS4100 accuracy values [50].

| Direction | Accuracy |
|----------------|----------------------|
| X and Y | <i>2% Dim</i> |
| Z | <i>0.2 + Dim/100</i> |

3.1.2 SAMPLES

The test sample must represent the population being examined and a consistent procedure must be used for its production, since material properties, hence the test results, are dependent on how the material was formed.

The provided polymeric samples were injection molded with 6mm thickness, using four different materials: pure PC, pure ABS and two PC/ABS blends in the ratios of 80:20 and 70:30. Mechanical properties, manufacturer and resin name are presented in Tab. 3.5. Tensile Yield Strength, σ_y , and Young's Module were obtained from manufacturers data sheet [51–54] while Poisson's ratio was retrieved from [55] and adopted for all polymers.

Table 3.5: Mechanical properties of the polymeric materials.

| Materials | Supplier | Resin Name | E [MPa] | σ_y [MPa] | ν |
|---------------------|----------|----------------------|---------|------------------|-------|
| PC | SABIC® | Lexan 243R | 2340 | 62 | 0.35 |
| PC/ABS 80:20 | INEOS® | Novodur Ultra 4140PG | 2100 | 46 | 0.35 |
| PC/ABS 70:30 | Ravago® | Mablex PCA | 2400 | 50 | 0.35 |
| ABS | INEOS® | Terluran GP-35 | 2300 | 44 | 0.35 |

The first step was the preparation of the samples, ensuring a 5mm thickness sample with flat and homogeneous top surface with similar roughness and no grinding defects. In order to achieve this, a metallographic grinding and polishing machine was used with different wet sandpaper grits and a polishing disk. Starting with a 120 grit wet sandpaper disc placed over the rubber disk and secured with appropriate cover.

The thickness was gradually reduced from both sides and constantly inspected with the vernier caliper. Upon reaching the desired thickness, as shown in Fig. 3.4, any sample that



Figure 3.4: Thickness comparison of PC samples.

presented residual error from the injection molding process (see Sec. 3.3.1) was replaced by a new one.



(a) Grit 120.



(b) Polished.

Figure 3.5: Surface finish of PC samples.

Once the first grit was concluded the sample was dried using paper towels, both surfaces were visually inspected and one chosen as test surface. A finer grit sandpaper was placed and the test surface repeatedly sanded, smoothing grinding marks until 1200 grit was reached. Then the rubber disk was replaced by a polishing disk and the surface was polished using alumina solution, Fig. 3.5 shows the obtained surface finish after thickness reduction (a) and polishing (b). The sample was then cleaned in running water, dried again and individually placed in a zip-lock bag with a paper label indicating its material, id and test load.

3.2 TESTING PROCEDURE

In possession of the prepared samples, the two hardness testing methods were carried out on four samples for each material to a better characterization of the materials. Three spaced measurements were taken in each sample quadrant near the corners, preserving the center for the indentation test.

At first tests were executed with DuraScan 20 applying a 0.1N load through a Vickers micro-indenter, shown in Fig. 3.6a. Then, Brinell Hardness tests were performed using an Universal Hardness Machine with a 2.5mm diameter tungsten carbide sphere and a 300N load, as represented in Fig. 3.6b. The first test intends to capture hardness variations on the

top layer, indicating a possible non-homogeneous surface [3]. These tests provides information on materials superficial resistance to penetrations with small loads.

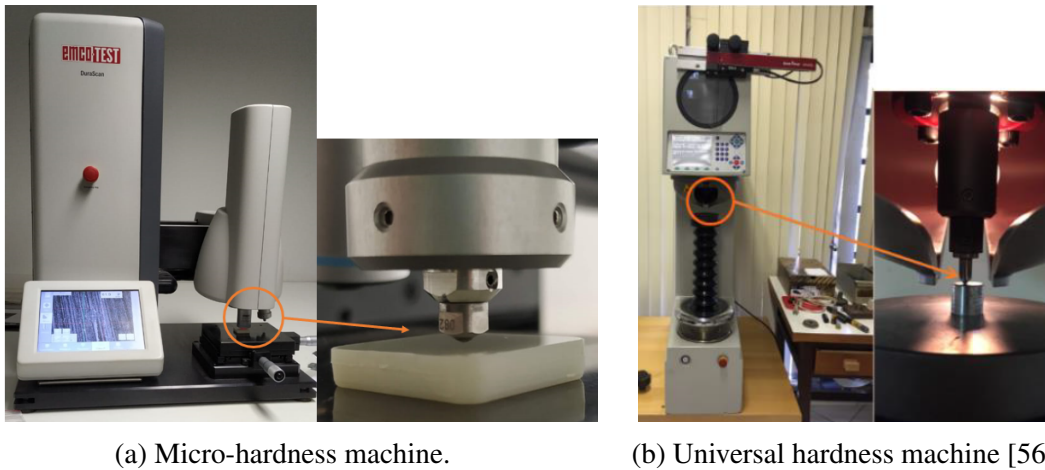


Figure 3.6: Hardness testing devices.

Afterwards, the sample is placed inside the holder device, which is closed with the lid, then bolted. On the MTS Landmark®, an indenter is positioned in the upper collet-grip and the closed device on the bottom one, as illustrated in Fig. 3.7. Then the cross-head was carefully lowered in such way as a small gap remains between the pad tip and sample, to ensure there was no damage. The cross-head was locked once the final position has been reached. With all the hardware in place the test was programmed for a 0.5mm/s displacement ratio until the specified load was attained.

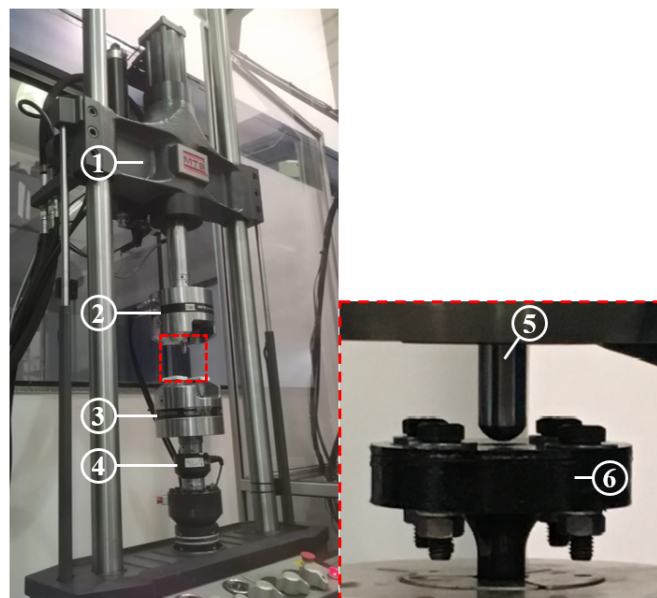


Figure 3.7: Test machine and components: 1) Crosshead, 2) Upper Collet-Grip, 3) Bottom Collet-Grip, 4) Load Transducer, 5) Indenter, 6) Holder Device.

Before the start of each test the axial displacement and load detectors limits were checked, as well as the crosshead and grip locks. Four load limits were defined: 500N,

1000N, 1500N and 2000N, and two tests done on each one for the studied materials. Every load-displacement curve acquired along the loading procedure were used to track tests progress and documented afterwards in a csv extension file. Due to the COVID-19 pandemic six tests on PC, whose data were not properly exported, couldn't be rerun and only 1500N load-displacement curves are presented. Once tests were completed and setup disassembled the test samples were stored.

As final step the confocal microscope was used to obtain the marks profiles, allowing the measuring process. As shown in Fig. 3.8, each sample was positioned on the microscope and chosen magnification varied between 10X and 20X objective lenses, depending on the marks size. Next, the brightness level was defined depending on the material aspect, to guarantee a proper lightning of the mark and the sample surface.

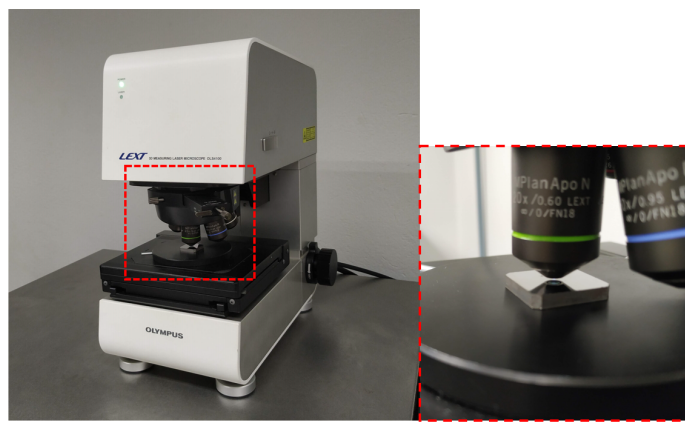
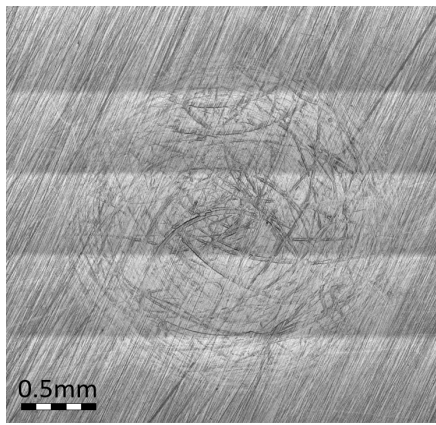


Figure 3.8: Sample positioning on the confocal microscope.

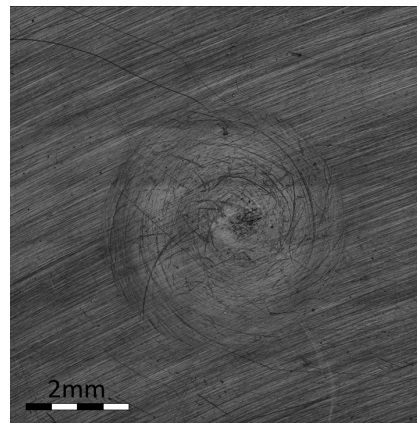
Then the scan range is set, the Z height manually varied upward and downward from the height with the best focus until all visualization is lost to guarantee that the mark will be scanned in its integrity. These positions are the top and bottom designations and were respectively given at locations above the specimens top surface, at a zone unaffected by the indentation, and below the center of the mark. The last item defined was the step height, determining the number of divisions of the scan range.

The scanning stage is fulfilled several times to provide final result as the applied magnification was not able capture the full mark. Parts captured in both laser and color spectrum were merged through stitching along the process and complete results were opened at the measurement environment. Figures 3.9a and 3.9b exemplifies the images obtained, they were obtained from ABS samples respectively tested with 500N and 2000N. Besides the marks, its possible to see the pattern created by the stitching process, the residual scars from the sanding stage during the preparation and also the impressions on the mark, generated from the indenter surface.

A line indicates the cross-sectional profile displayed, and is moved to show he profile at the highest diameter. Before the measurements were taken surface correction was applied to compensate deviations on XY Plane and noise filter applied to smooth the obtained pro-



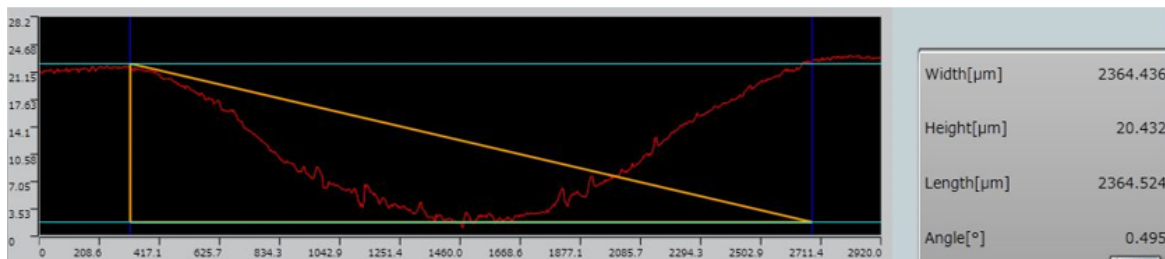
(a) 500N, 20X.



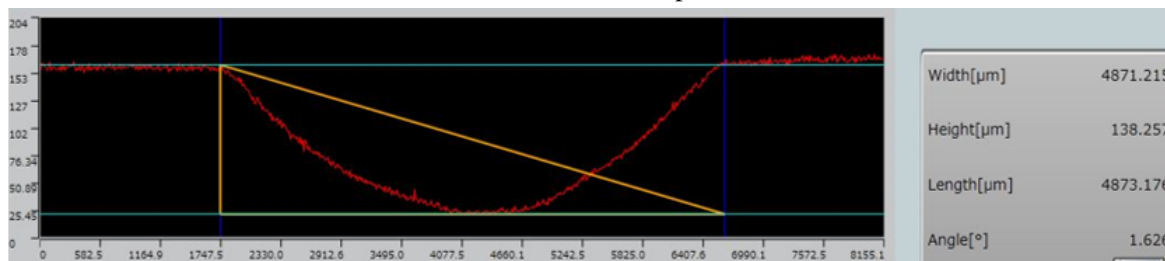
(b) 2000N, 10X.

Figure 3.9: Stitched images of indentation marks on ABS samples (Load, Magnification).

files, allowing easier and more precise measurements using the tool, with two horizontal and vertical lines.



(a) 500N test sample.



(b) 2000N test sample.

Figure 3.10: 2D profiles of indentation marks on ABS samples.

Figure 3.10 shows the treated profiles for the indentation marks presented above. The measuring tool lines were aligned with the mark geometry, measurements were taken on both Y and X directions in order to capture possible eccentricities. The profile in Fig. 3.10a shows that the applied noise filter still maintains the scars in the mark's surface and in Fig. 3.10b the profile is slightly asymmetrical, which might be a consequence of the surface correction applied. A detailed procedural algorithm is available in 5.2.

3.3 UNCERTAINTY ANALYSIS

Once experimental procedure was established the associated uncertainty sources were identified, three main groups are discussed in the following subsections: manufacture errors, repeatability and measurement uncertainties. This process was performed following experimental methodology sequence to correctly address each identified source and individual contributions.

3.3.1 MANUFACTURE ERRORS

Injection molding is the process most used to mold thermoplastic materials and was by this process that the samples tested in this study have been produced. Simply describing, it starts by preheating the polymer pellets in a chamber until the melt temperature is attained and then it is forced into the closed mold cavity through considerably high pressures. Usually this pressure is generated by a reciprocating screw, that serves two main purposes: providing the molten polymer mass and force it into the mold, that is at a lower temperature [19].

Despite the simple description of the process it has been constantly evolving with the technological advances from the last decades, achieving high-end machines that have different means of controlling the molding cycle, detailed in Fig. 3.11 [57].

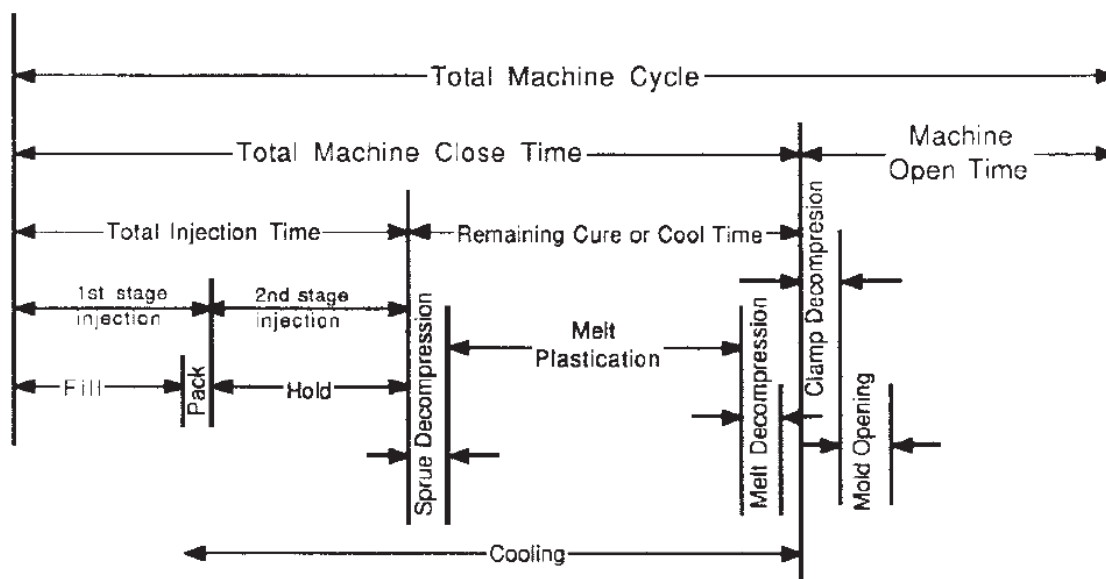


Figure 3.11: Molding cycle components, extracted from [57].

Although the hole process exerts direct influence at the specimens and its properties, consequently affecting the test results. The most important step to control is the injection one, and the best way to have consistent test specimens is by an automatic cycle with the correct control of its parameters. Among the many influence factors there are: geometry, size and temperature of the heating chamber, pressures and speeds used, cavity layout, tolerance

and surface finish, mold temperature and its uniformity and timing cycles used [57].

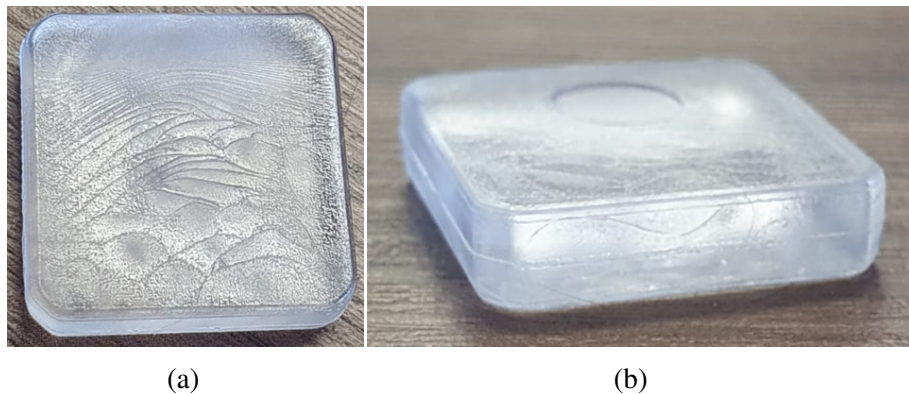


Figure 3.12: Manufacture errors in PC samples.

The mold is one of the critical variables affecting the specimen properties and its cavities must have the appropriate tolerances depending on the material to be molded and the test methods. Fig. 3.12 shows examples of the manufacture errors in the samples received, in (a) the rough surface finish and shrinkage are evidenced by the present lines and their convergence towards the top edge; in (b) the opposite side is shown, containing the same surface finish, presence of weld lines and the circular marks from the ejector pins.

Due to all possible variability a Standard Practice for Injection Molding Test Specimens of Thermoplastic Molding and Extrusion Materials, ASTM D3641-02, was developed and covers the general guidelines to be followed. It clearly states that all conditions might vary for each thermoplastic and if the material standard is not available, does not contain the molding conditions or differ from material specification the supplier recommendations must be considered [57].

Besides all possible variability from the manufacturing process, polymers might present quite high variability of its properties for different batches of the same material [46]. With that being said, it is of great importance to highlight that the samples tested for each material were from the same batch, manufactured by a third-party and, as previously mentioned, pellets came from different suppliers. Blends ratios are known but no information regarding each PC and ABS composition were provided nor manufacturing specifications, besides being injected molded.

3.3.2 REPEATABILITY

Throughout the study, some general sources of variation had been identified and will be addressed here. As this is a preliminary study of the materials being tested and the main focus was the methodology in use, some good practices of experimental procedures were neglected. Some of them, like the number of tests for each configuration and the use of different suppliers, were totally intentional, while others happened due to incorrect assumptions.

There is no specific standard for general indentation tests, so the ones referring to hardness tests are the closest available. A standard was created to address the specification for multipurpose plastic test specimens, the ASTM D5936-96, but it was withdrawn in 1998 with no replacement. Taking that in consideration the best course of action is to have the final test methodology in accordance to the standard for Rockwell hardness tests of plastics.

Since the sample holder device was created as an adaptation to amplify the use of the test machines available, and was not strictly focused on polymer testing, the current allowable thickness is smaller than the value specified by ASTM D785-03. As previously indicated in the methodology, the sample preparation serves two purposes, but as the process is highly manual it allows variations for the thickness and the parallelism of the surfaces. The effect over the surface parallelism is exemplified by the profiles measurements in Fig. 3.10, the measurement tool also provides the surface angle, which varied between 0.029 and 1.626° .

Based on the manufacturing process of the indenters a deviation of $\pm 0.1\text{mm}$ is expected, Fig. 3.13a shows the side view an indenter tip. They had machined surface finish and were only inspected visually, the ones presenting major surface defects were discarded. Fig. 3.13b shows the surface finish of an approved indenter, but ideally they should be further prepared to obtain a polished surface finish and have all dimensions evaluated.

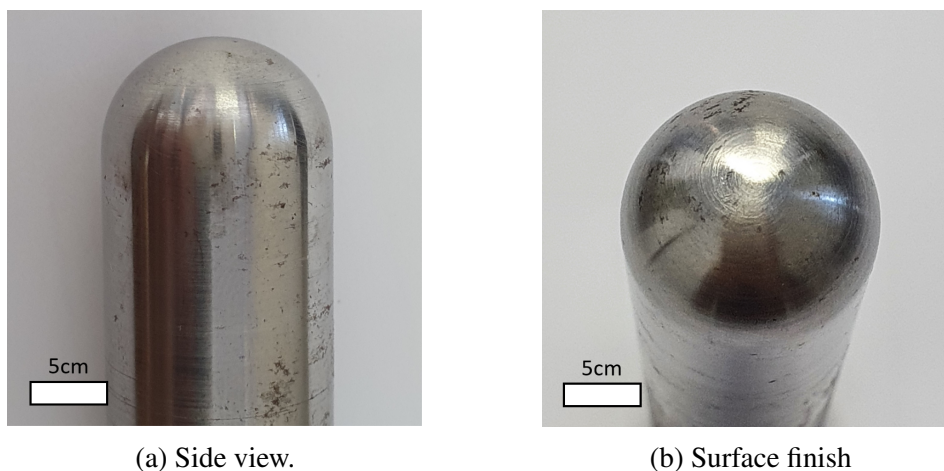


Figure 3.13: Example of an approved indenter tip.

The test setup allowed variations of the gap between the tip of the indenter and the specimens surface. Prior to the results analysis, the only effect considered for this residual distance was the test duration, which was deemed as not relevant and will be further discussed at Sec. 4.2.

3.3.3 MEASUREMENT UNCERTAINTIES

From the indentation test onward, equipment accuracy and other uncertainty sources directly affects the measurements taken. A thorough evaluation was performed to identify, quantify and combine these sources for load and indentation impression geometry measure-

ments. The flowchart shown in Fig. 3.14 presents the general analysis process to obtain the individual uncertainty values affecting the variable of interest, and processing them to quantify their influence.

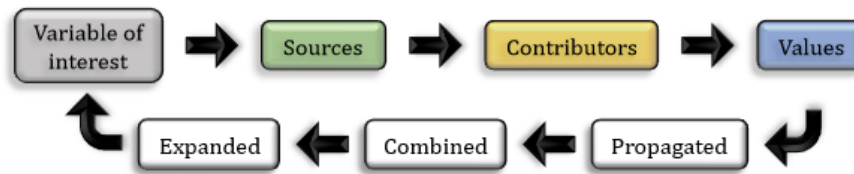


Figure 3.14: Uncertainty analysis flowchart.

Once the sources are identified, their individual contributions are investigated and defined using statistics or other sources, like past experience, experimental investigation, calibration reports, published information or manufacturer’s specifications [44].

Once the different uncertainty contributions (U_i) are calculated, they can be combined by the root sum of squares (RSS), as represented by Eq. (3.2). The result is called combined uncertainty (CU).

$$CU = \sqrt{\sum_{i=1}^n U_i^2} \quad (3.2)$$

The combined uncertainty may be considered as equivalent to a standard deviation, requiring it to be re-scaled to obtain another level of confidence. The result is called the expanded uncertainty, EU , calculated by:

$$EU = k \times CU \quad (3.3)$$

where k is the coverage factor. Most commonly the value of the coverage factor $k = 2$ is used to give a level of confidence of approximately 95%, assuming a normal distribution for the combined uncertainty [43].

As the discussed sources related to the measuring procedure, averaging also brings a component to be taken into account known as the standard uncertainty of the mean (U_{std}). Its contribution is given as function of the estimated standard deviation (s), which represents the spread of values, and the number of measurements taken (n):

$$U_{std} = \frac{s}{\sqrt{n}} \quad (3.4)$$

- Load

Load readings were obtained from the tests fulfilled on the MTS Landmark®, becoming the most relevant equipment and presenting relationship with the uncertainty

sources. From the identified sources, three of them contained quantifiable components: load transducer, testing machine and data noise. Figure 3.15 shows the identified sources and related uncertainties. Whenever multiple individual contributors were identified for an individual source they were combined using RSS, which is represented by curly braces in the flowcharts presented.

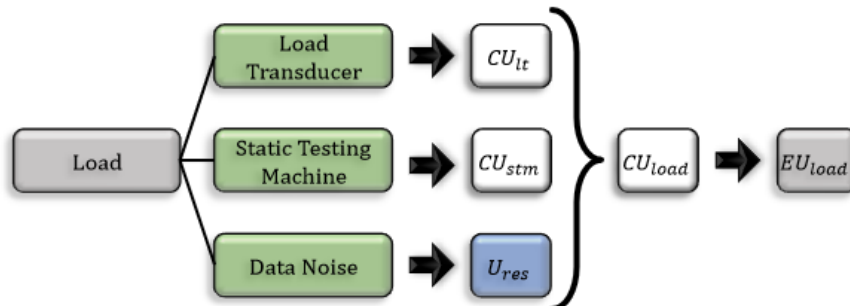


Figure 3.15: Uncertainties flowchart for the load.

Starting with the load transducer, three individual components were identified and accounted for, which were combined into CU_{lt} and expanded to EU_{lt} as shown in Fig. 3.16.

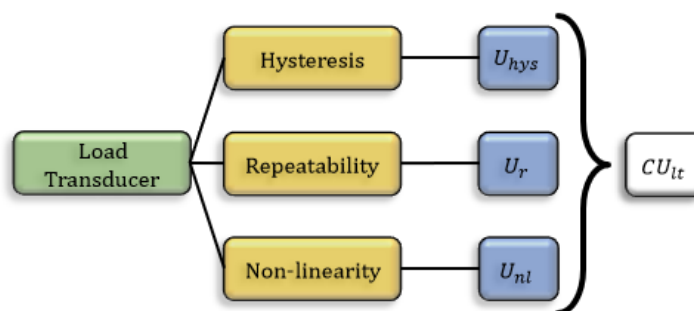


Figure 3.16: Uncertainties flowchart for the load transducer.

The individual components are: hysteresis (U_{hys}), repeatability (U_r) and non-linearity (U_{nl}). They were identified from the equipment specification, provided by its manufacturer, are defined in function of the device full scale as shown in Tab. 3.2 and were combined using Eq. (3.5).

$$CU_{lt} = \sqrt{U_{hys}^2 + U_r^2 + U_{nl}^2} \quad (3.5)$$

As previously mentioned the testing machine might contain several uncertainty components, even in its static state, represented by the static testing machine combined uncertainty (CU_{stm}). Fig. 3.17 shows two components, the uncorrected error uncertainty (U_{ue}) and the machine repeatability uncertainty (U_{rep}).

Testing machines force-measuring system should be calibrated and verified periodically, ISO 7500-01(E) [58] provides a standardized procedure. During this procedure it is common to leave a small uncorrected error, which won't compromise the machine

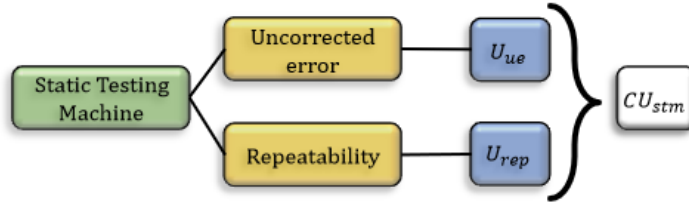


Figure 3.17: Uncertainties flowchart for the static testing machine.

functionality. Its value is indicated into the calibration report and must be considered during the analysis, the last calibration of the testing machine in use reported the values presented in Tab. 3.1 and is represented by U_{ue} .

As indentation tests were carried out with constant true force as stop condition, each load level presented an indicated force (F_i) as final data point. With n being the number of tests and \bar{F} the averaged indicated force, Eq. (3.6), retrieved from ISO 7500-01(E) [58], gives the repeatability uncertainty in percentage of the nominal force, F_n , and Eq. (3.7) the value in Newtons.

$$u_{rep} = \frac{1}{\sqrt{n}} \left(\frac{100}{\bar{F}} \sqrt{\frac{1}{(n-1)} \sum_{i=1}^n (F_i - \bar{F})^2} \right) \quad (3.6)$$

$$U_{rep} = \frac{u_{rep}}{100} F_n \quad (3.7)$$

In this study the uncorrected error, U_{ue} , given by previous calibration report, and the calculated component for the repeatability, U_{rep} , were combined using Eq. (3.8), giving the basal uncertainty for each load level.

$$CU_{stm} = \sqrt{U_{ue}^2 + U_{rep}^2} \quad (3.8)$$

Resolution uncertainty occurs due to variation of readings during machine use. Its defined as function of one increment of the numerical indicator or, if load readings shows fluctuations higher than one increment, it is considered equal to half the range of the registered fluctuation. During the inspection of the exported data, it was noticed that many tests presented major fluctuation, or noise, while the actuator traveled along the remaining gap, providing meaningless data. To properly address this issue a data treatment was necessary, process described in Sec. 3.4, and U_{res} was deemed as function of noise range (N_{rg}), defined by the relationship:

$$U_{res} = \frac{N_{rg}}{2} \quad (3.9)$$

The load combined uncertainty was finally calculated for every point of data sets using

the following equation:

$$CU_{load} = \sqrt{CU_{lt}^2 + CU_{stm}^2 + U_{res}^2} \quad (3.10)$$

During the analysis, the expanded uncertainty for the load, EU_{load} , was obtained to represent the uncertainty envelope. Once the polynomial regression of the experimental data was performed, the residuals were analyzed and the coverage factor calculated so that the combined uncertainty was expanded to cover 95% of the residuals.

- Impression Diameter and Depth

Once the measurements were taken during microscopic analysis, their uncertainty was calculated, following the general steps shown in Fig. 3.18. Since the same equipment and procedure were applied for the measurement of indentation diameter (d) and depth (h), they contained the same uncertainty components and both are treated as 'dim' in the flowchart and equations presented.

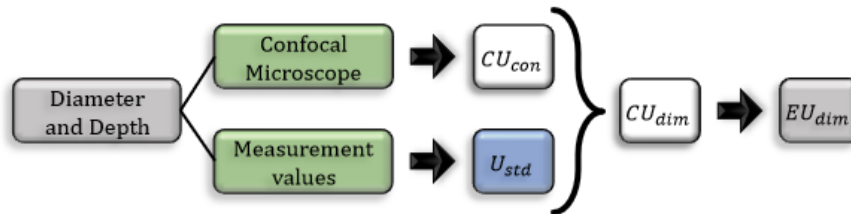


Figure 3.18: Uncertainties flowchart for the indentation diameter and depth.

As said in Sec. 3.1.1, the confocal microscope possesses an accuracy uncertainty (u_{acc}), relations presented in Tab. 3.4, and an additional uncertainty was adopted for the measurement tool (u_{mt}), assumed as 5% of the measurement. The confocal combined uncertainty (CU_{con}) was obtained as indicated in Fig. 3.19.

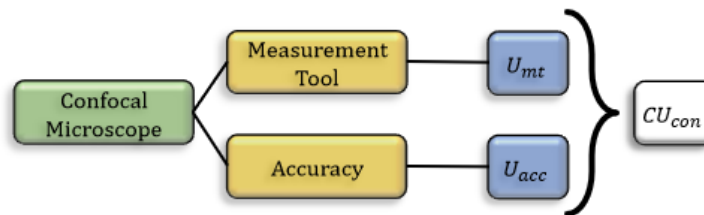


Figure 3.19: Uncertainties flowchart for the confocal microscope.

To obtain a single value, for either depth and diameter of the indentation impression at each load level, measured values from microscopic inspection were averaged and errors propagated and combined. As measurements taken on X and Y directions has individual uncertainties (u_i) they were propagated through the mean, using the equa-

tion:

$$U_{mean} = \frac{1}{n} \sqrt{\sum_{i=1}^n u(i)^2} \quad (3.11)$$

Thus, applying Eq. (3.11) to propagate the individual contributions, the following equations were obtained for the accuracy uncertainty (u_{acc}) and the measurement tool uncertainty (U_{mt}):

$$U_{acc} = \frac{1}{n} \sqrt{\sum_{i=1}^n u_{acc}(i)^2} \quad (3.12)$$

$$U_{mt} = \frac{1}{n} \sqrt{\sum_{i=1}^n u_{mt}(i)^2} \quad (3.13)$$

In order to quantify the confocal microscope contribution on the measurements, the considered contributions were combined into CU_{con} :

$$CU_{con} = \sqrt{U_{acc}^2 + U_{mt}^2} \quad (3.14)$$

The combined uncertainty for indentation diameter, CU_d , and depth, CU_h , can be calculated by Eq. (3.15), with the respective values obtained for the confocal combined uncertainty (CU_{con}) and the standard uncertainty of the mean U_{std} , obtained through Eq. (3.4).

$$CU_{dim} = \sqrt{U_{std}^2 + CU_{con}^2} \quad (3.15)$$

From the values calculated for the combined uncertainty of the diameter, depth, the expanded uncertainties (EU_d and EU_h) were obtained using a coverage factor $k = 2$.

3.4 DATA TREATMENT

Starting the data analysis several issues were noticed: large and non-uniform data sets, different initial actuator position, meaningless load readings until gap was closed. These issues were caused by: small sample rate frequency definition, uneven gap among tests, uneven initial actuator position and load noise with varied mean and amplitude.

Figure 3.20 shows an example of the raw data collected only for the loading stage, all images used as example and consequentially the values presented in this section were obtained from specimen F5, made of PC/ABS 70:30 and used at a 2kN test. In this specific

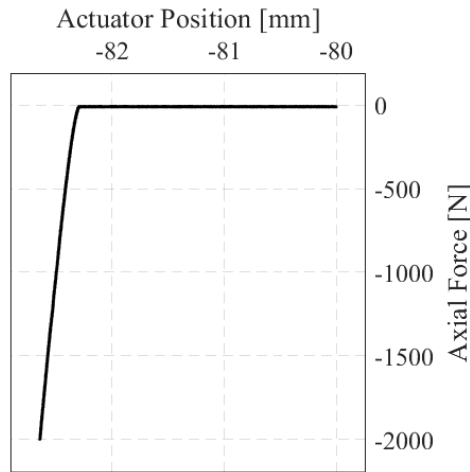


Figure 3.20: Raw data example for a PC/ABS 70:30 test at 2kN.

test, the initial actuator position was -80mm, with a total travel of 2.65mm and estimated gap of 2.3mm. The number of data points captured was 32058, with average noise (N_{avg}) of -9.57N and noise range (N_{rg}) of 3.7N.

As mentioned the initial part of the collected data ended up being meaningless, not only due to noise captured but also due to the running-in stage. In order to filter the steady-state stage data a load cutoff was defined as shown in Eq. (3.16), taking into account the average noise (N_{avg}), the load transducer combined uncertainty (CU_{lt}) and the lower value of the static testing machine combined uncertainty (CU_{stm}). Instead of using a fixed value as threshold, this method was preferred due to the variation of the captured noise, being able to treat each data set according to its specificity using a standardized process.

$$Cutoff = N_{avg} - \sqrt{CU_{lt}^2 + CU_{stm}^2} = N_{avg} - 5.1 \quad (3.16)$$

The first data point was selected once all subsequent values were lower than the applied variable cutoff. Figure 3.21 shows the noise treatment applied on the data set used as example. From the total data 27840 were deemed as noise, with the first data selected at -82.30mm and -15.40N.

After the noise treatment, the raw data was divided into noise and valid data and there was a total of 4218 data points left, from which 50, 100, 150 or 200 were evenly selected to compose the final data, as shown in Fig. 3.22a, depending on the load range.

The last issue to be addressed was the different initial position of the actuator. The final displacement-force curves, similar to Fig.3.22b, were normalized by subtracting the values of the first selected data point from all selected data.

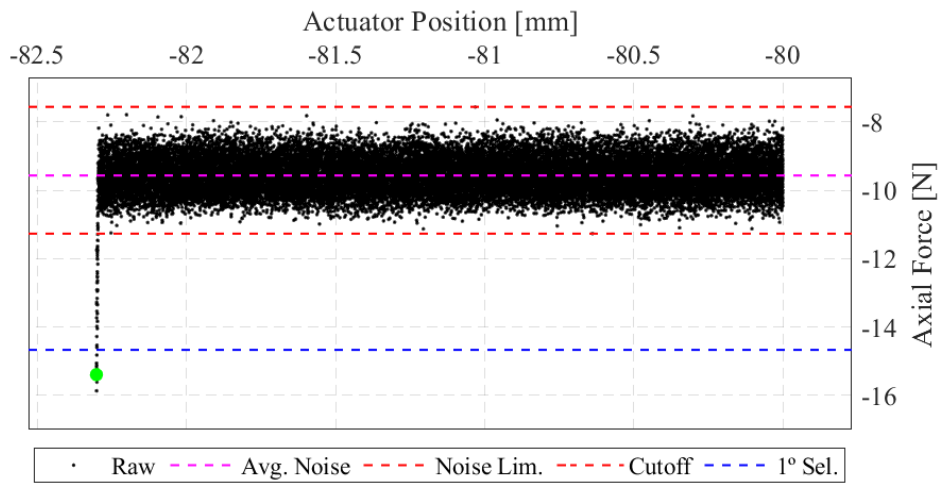


Figure 3.21: Noise handling example for a PC/ABS 70:30 test at 2kN.

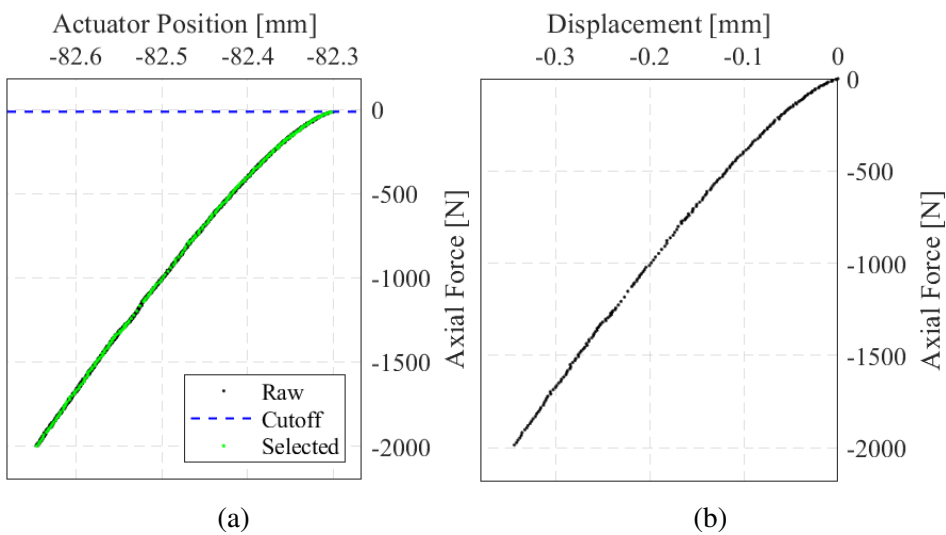


Figure 3.22: (a) Data sampling and (b) final data examples for a PC/ABS 70:30 test at 2kN.

Chapter 4

RESULTS AND DISCUSSION

Based on the concepts and methodologies presented in Chapters 2 and 3 all results of this study were directly or indirectly obtained and are presented in five sections. The first one contains the analytical results obtained using the Hertzian formulae, providing an estimate for key-values at yield, followed by the second section providing the results of the indentation tests, that consists of: a presentation of values related to the raw data and the applied treatment, the load-displacement curves collected

It is followed by the microscopic analysis results showing, for each tested configuration the average measurements of the diameter and depth of the indentation marks. The fourth section contains the results for the two standard hardness testing methods performed on the four materials in study, as well as an approximation for Brinell hardness, using the measurements of the indentation marks, with a discussion of the size-scale effect.

The fifth section contains the quantified uncertainties with their respective individual components, for the three variables of interest, as well as an analysis in order to identify the major contributors. Closing this chapter the average behavior of the materials is obtained from polynomial regressions and a residual analysis is carried out to evaluate the goodness of fit.

4.1 HERTZIAN SOLUTION

Material properties presented in Tab. 3.5, given by manufacturers datasheet, were obtained from tensile tests. Assuming an isotropic behavior of the materials the Hertzian solution was used to obtain expected values at yield for: maximum contact pressure (p_0), Load (P), half-length of the contact arch (a) and indenter displacement (δ).

Equations (2.4) and (2.5) provides the stresses along the symmetry axis, shown in Fig. 4.1, which are the higher values. The maximum value of $|\sigma_z - \sigma_r|$, for $\nu=0.35$, is $0.597p_0$ at a depth of approximately $0.50a$. Thus by the von Mises criterion a relation is obtained for the maximum contact pressure and the yield strength: $p_0 = 1.67\sigma_y$.

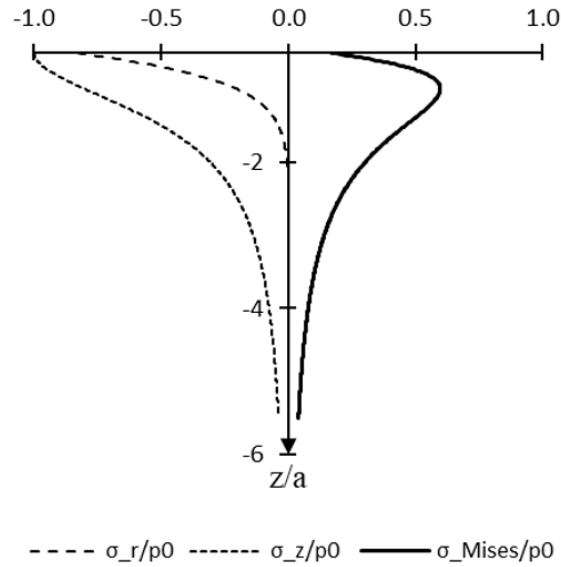


Figure 4.1: Stresses along the axis of symmetry for $\nu = 0.35$.

Results obtained are presented in Tab. 4.1, since the indentation tests provides load-displacement curves, these results are the most relevant.

Table 4.1: Hertz solution results at yield.

| Material | E^* [MPa] | p_0 [MPa] | P [N] | a [mm] | δ [mm] |
|--------------|-------------|-------------|---------|----------|---------------|
| PC | 2636.63 | 103.80 | 46.77 | 0.464 | 0.029 |
| PC/ABS 80:20 | 2368.94 | 77.01 | 23.66 | 0.383 | 0.020 |
| PC/ABS 70:30 | 2703.45 | 83.71 | 23.33 | 0.365 | 0.018 |
| ABS | 2592.06 | 73.66 | 17.29 | 0.335 | 0.015 |

It is visible from the results that both blends showed very similar values for all variables. The higher results were obtained for PC and ABS have the smaller values, which is counter-intuitive since ABS is more ductile and mostly for the displacement, higher values were expected. A closer evaluation of the material properties, shown in Tab. 3.5, reveals that the yield strength (σ_y) of PC is 40% higher than ABS', which explain the achieved results.

From displacement results it was noticed that for this configurations yield is expected to occur briefly after contact is closed. Since loads at yield stays within dozens of Newtons the elastic regime might not be properly captured, due to test machine uncertainties and the mentioned repeatability errors in the methodology. In addition to these factors there is also great uncertainty related to the material behavior, for being viscoelastic and since higher strength values are expected under compression, as discussed in Sec. 2.2.2.

Overall the identified limitations does not impact the purpose of this study, our interest lies in the methodology and uncertainties related to indentation tests using loads in the order of hundreds and thousands of newtons, causing high inelastic deformations and leaving the scope of the analytical solution.

4.2 INDENTATION RESULTS

4.2.1 DATA TREATMENT

As previously mentioned, the sampling rate applied during the indentation tests was excessive. In some cases collected data was long, captured noise and was not sequential. Through the data treatment described, the majority noise was removed, data sets were shortened, obtaining a sequential order and remaining in great accordance with raw data.

Table 4.2 presents minimum and maximum values for some indicators collected in the process, exemplifying the necessity of the treatment. From the number of data and valid points its evident how long and uneven the data sets are. The number of noise points shows the inconsistency of the gap left between the indenter and sample with very different cutoff values, to compensate the different behavior of the noise captured.

Table 4.2: Maximum and minimum values of indicators for the data treatment.

| | #Data | #Noise | #Valid | Cutoff [N] | N_{avg} [N] | NRG [N] |
|------------|-------|--------|--------|------------|---------------|-----------|
| Min | 358 | 19 | 255 | -1.90 | 3.20 | 3.14 |
| Max | 41502 | 39513 | 6757 | -15.08 | -9.98 | 9.14 |

From the noise average (N_{avg}) and range (N_{rng}) values its clear that they not only showed major variation. Even tough the effect over test run time was irrelevant, since load limit was attained in a matter of minutes, the load noise captured during the uneven gap travel hid the exact moment of contact establishment. Since the running-in stage is usually despised, the effect of the applied cutoff over the measured displacement was not taken into account.

4.2.2 LOAD-DISPLACEMENT CURVES

Charts were created with the treated data and are presented in Fig. 4.2. including all tests performed on each material.

The acquired curves for PC and PC/ABS 70:30, shown in Figs. 4.2a and 4.2c are the best results, presenting great fit among curves which indicates consistency on the tests procedures and material behavior among the tested samples. On the other hand the curves for PC/ABS 80:20, in Fig. 4.2b, are horizontally dislocated but presenting similar tendency. As for ABS results in Fig. 4.2d, there are two major distinctive aspects, being the two curves showing a different tendency and a abrupt change on the curves behavior. These inconsistent results can represent non-conformity of the tested samples.

Curves in 4.2d presented a change in its form for all tests with loads higher than 1000N, located at different displacement values for different tests representing approximately 7-11% of the specimen thickness. During microscopic inspection a whitened area, shown in Fig. 4.3, was noticed at the bottom surface of the samples of these tests.

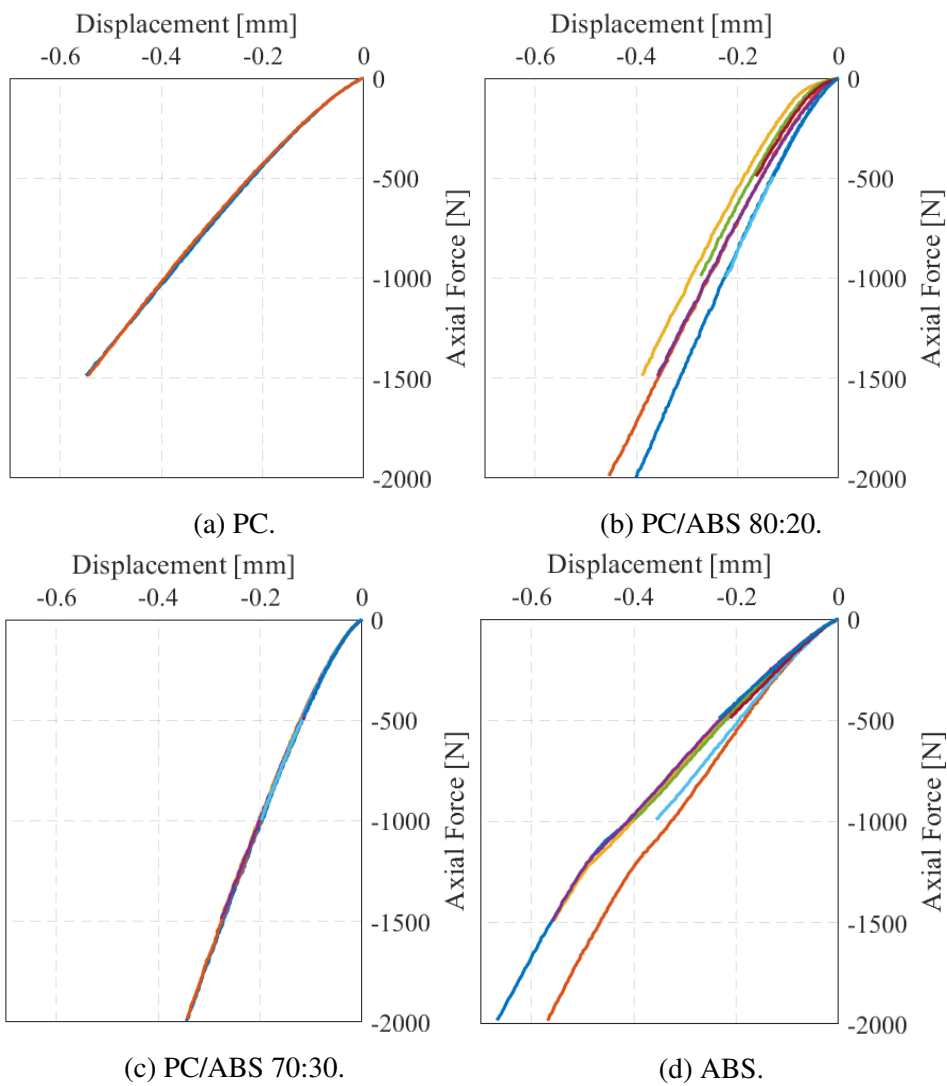


Figure 4.2: Load-displacement curves collected during indentation tests.

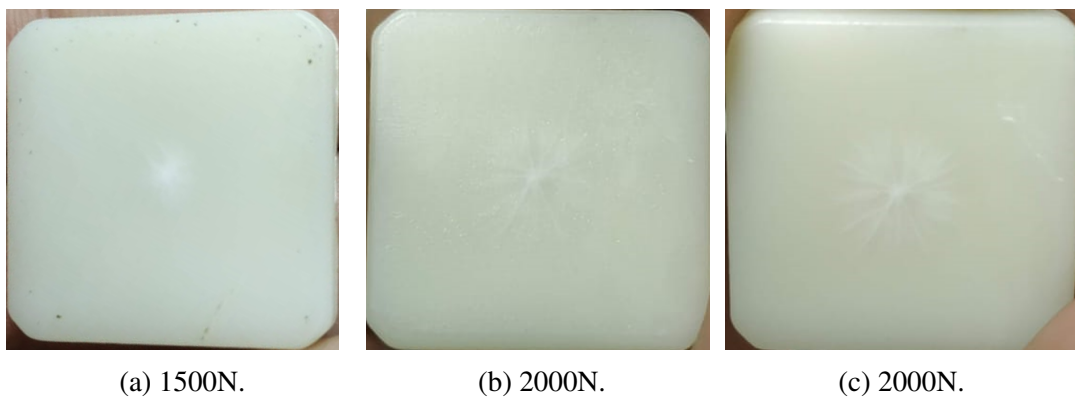


Figure 4.3: Whitened area at the bottom surface of ABS samples.

They have the aspect of radial cracks, they are presumed to be crazes, which are bridged cracks capable to withstand loading. They are common in tensile tests, being located in the neck and responsible for its stable propagation but as the stress field during indentation is complex, this region might present tensile components during deformation. This indicates

that stress magnitude was enough to make the field exceed the specimen thickness, initiating material failure, and the insufficient thickness is related to the change in curves behavior.

Although being from different suppliers, mechanical properties obtained from manufacturers data sheet were relatively similar and describes the elastic regime under tensile stress. The presence of whitened area exclusively on ABS samples corroborates that ABS was the most ductile of the studied materials. From results obtained with the Hertzian solution shown in Tab. 4.1, indicating that yielding occurs at small loads and displacements for all materials, and the fact that the whitened region is seen only for ABS samples, two assumptions emerges: blending placed blends plastic behavior closer to PC's and tension-compression properties have very different values.

Despite the fact that plastics that don't fail by shattering fracture have an arbitrary value of compressive strength, which is the behavior for the tested materials, its value might be useful for comparison [18]. Further information regarding the plastic behavior of these specific resins, under compression, are necessary to fully comprehend the appearance of the whitened area and improve future studies.

4.3 MICROSCOPIC INSPECTION

The indentation impressions obtained, exemplified in Fig. 4.4, were inspected based on the methodology presented in Sec. 3.2. The circular marks on the top surface of the samples are from burrs of a thin edge of the device's top lid, where a groove was machined to contain an O-ring that acts with the rubber sheets to provide sample stabilization.

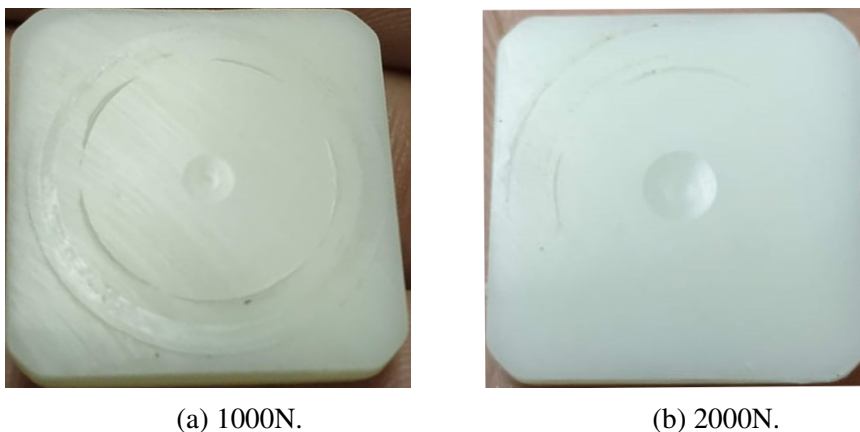
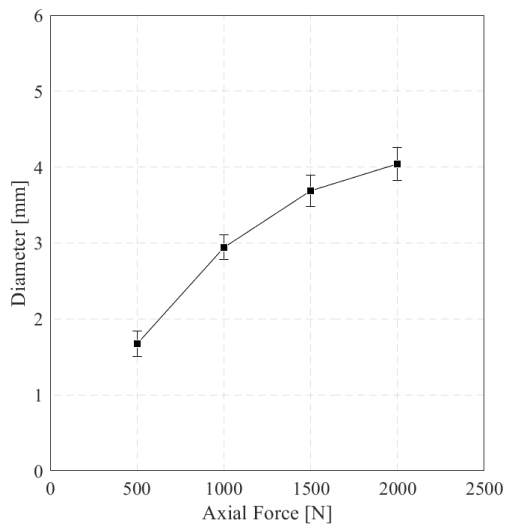


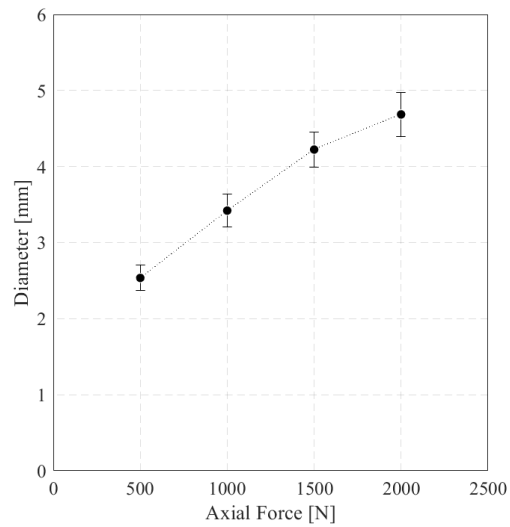
Figure 4.4: Indentation marks on ABS samples.

As mentioned, diameter and depth were measured on 2D profiles, from cross sections in X and Y directions of the scanned 3D model, and averaged to represent a single data point for each configuration on the respective plots. Average diameter for each material tested, with the respective uncertainties as error bars, are presented in Fig. 4.5.

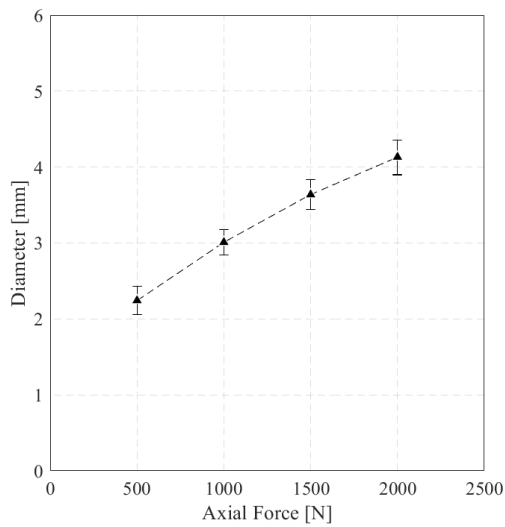
PC results in Fig. 4.5a showed the most distinct results, with a higher variation of



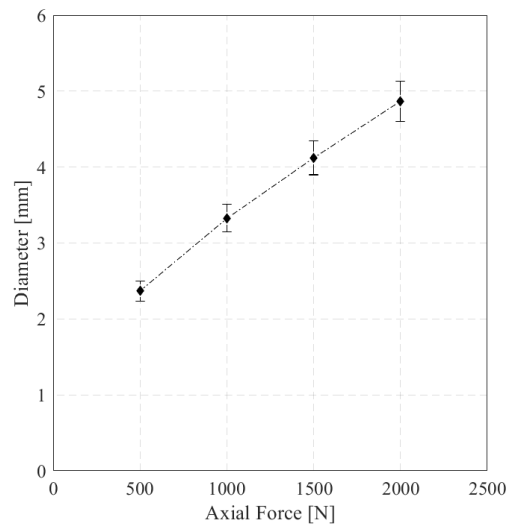
(a) PC.



(b) PC/ABS 80:20.



(c) PC/ABS 70:30.



(d) ABS.

Figure 4.5: Averaged measurements for indentation diameter.

the diameter-load response which presents a lower increase of diameter as load increases. PC/ABS 80:20 in Fig. 4.5b shows a linear response for 500N, 1000N and 1500N that decays for 2000N. Average values for PC/ABS 70:30 and ABS, respectively shown in Figs. 4.5c and 4.5d shows an almost linear tendency with small deviations. Average results for all tested materials presents small estimated uncertainties.

For an general overview individual results were grouped in Fig. 4.6. Overall, as expected, diameter results shows a crescent tendency as load increases. PC showed the smaller average diameter for all load levels besides 1500N, although very similar for all loads, the 70:30 blend presented the smaller value for 1500N. Similarly to the lower values, higher values were obtained for the same material except for a single load level, the blend of 80:20 presented the higher values from 500N up to 1500N, being surpassed by ABS at 2000N. This fact might be attributed to the appearance of the whitened area, the failure process of ABS samples may have allowed greater deformations.

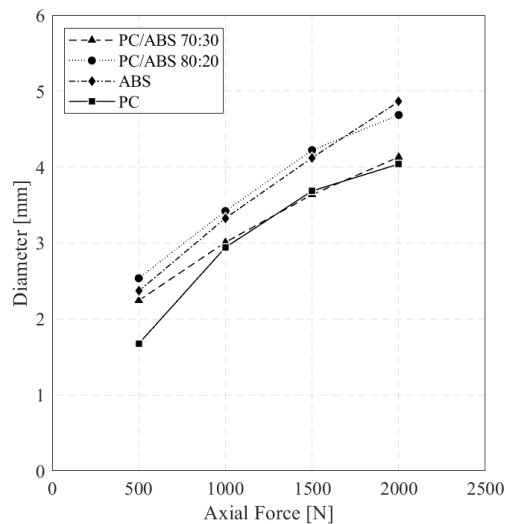


Figure 4.6: Grouped results for indentation diameter.

A last and unexpected observation from the obtained results is related to the similarity among materials. Once again results did not reflect the blending ratios, ABS and PC/ABS 80:20 showed similar values while PC's were closer to PC/ABS 70:30.

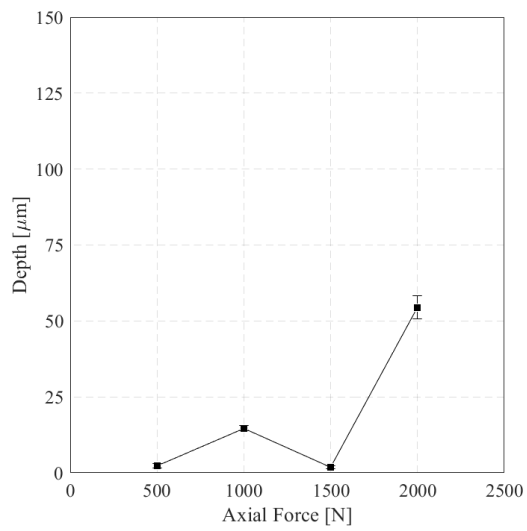
Similar plots were also obtained for depth average results for its analysis and are presented in Fig. 4.7.

Similarly to diameter results, indentation depth for PC shown in Fig. 4.7a have the most distinct behavior. The major difference emerges from the average value for 1500N due to an almost nonexistent depth, which was visible to the naked eye. Values for other load levels showed an expected response. Both samples were from the same batch and were prepared and tested following the same procedures, unfortunately the load-displacement curves showed in Fig. 4.2a were not captured for other load levels besides 1500N.

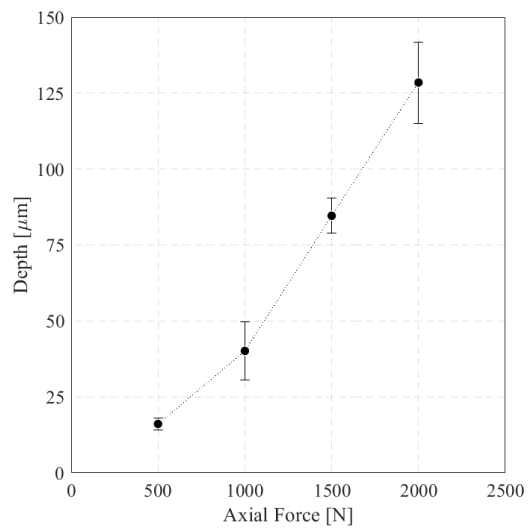
Average values for PC/ABS 80:20 in Fig. 4.7b shows a linear tendency for 1000N, 1500N and 2000N. As well as the disperse curves in Fig. 4.2b, depth measurements also showed higher variation as indicated by the error bars. Results for PC/ABS 70:30 in Fig. 4.7c presents the same behavior of the load-displacement curves in Fig. 4.2c with an accentuated increase from 1000N onward, entering in a linear tendency. Differently from the diameter results for ABS, depth values shown in Fig. 4.7d have the higher variation between load levels, observed at values for 1500N and 2000N.

The uncertainties estimated for depth shows great variation, being minimal for most conditions and higher for some load levels for the materials with the worst load-displacement curves.

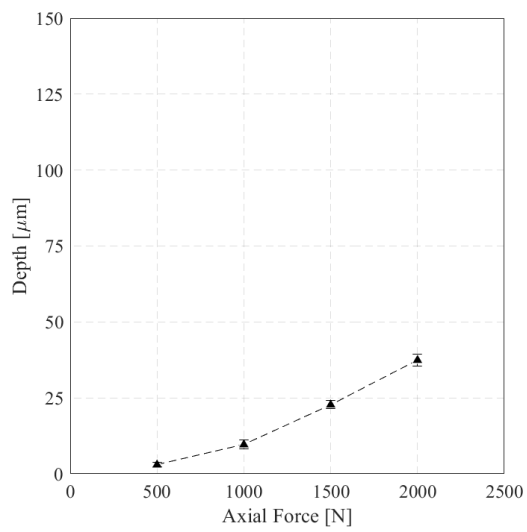
For a comparison among tested materials Fig. 4.8 presents all averaged depth results. The same unexpected pairing of materials observed for diameter results in 4.6 is seen, PC and PC/70:30 showed similar results while values for ABS were closer to PC/ABS 80:20. Minimum and maximum values varied between polymer and blends pairs. It was interesting



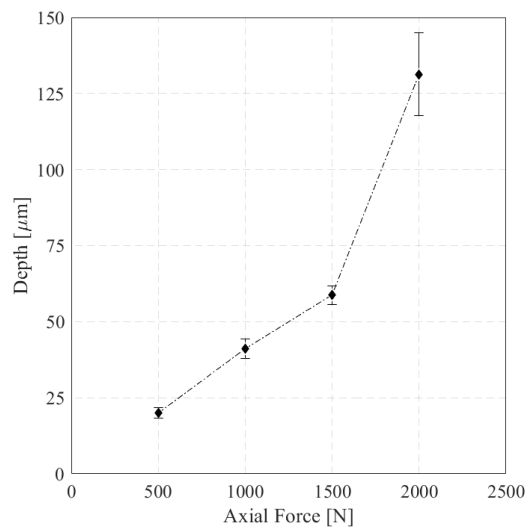
(a) PC.



(b) PC/ABS 80:20.



(c) PC/ABS 70:30.



(d) ABS.

Figure 4.7: Averaged measurements for indentation depth.

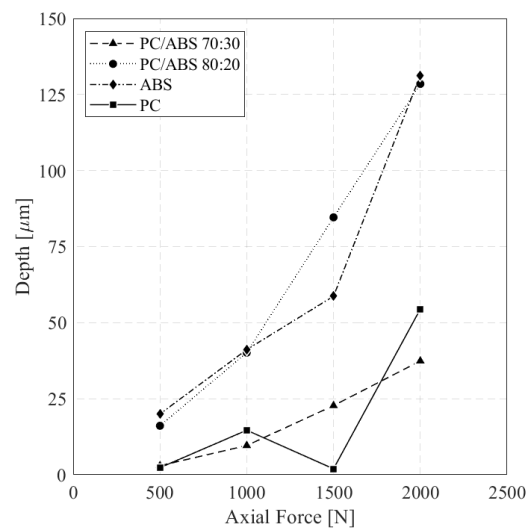


Figure 4.8: Grouped results for indentation depth.

to see that the maximum depth value for PC/ABS 70:30 was smaller than ABS and the blend 80:20 at 1000N.

The maximum displacement was extracted from the load-displacement curves, values averaged similarly to depth measurements. From the total displacement applied, material response generates the three different types of strain: elastic, visco-elastic and plastic. Figure 4.9 shows material recovery, presenting the total displacement (white markers), with the standard deviation as error bars, and the residual depth (black markers).

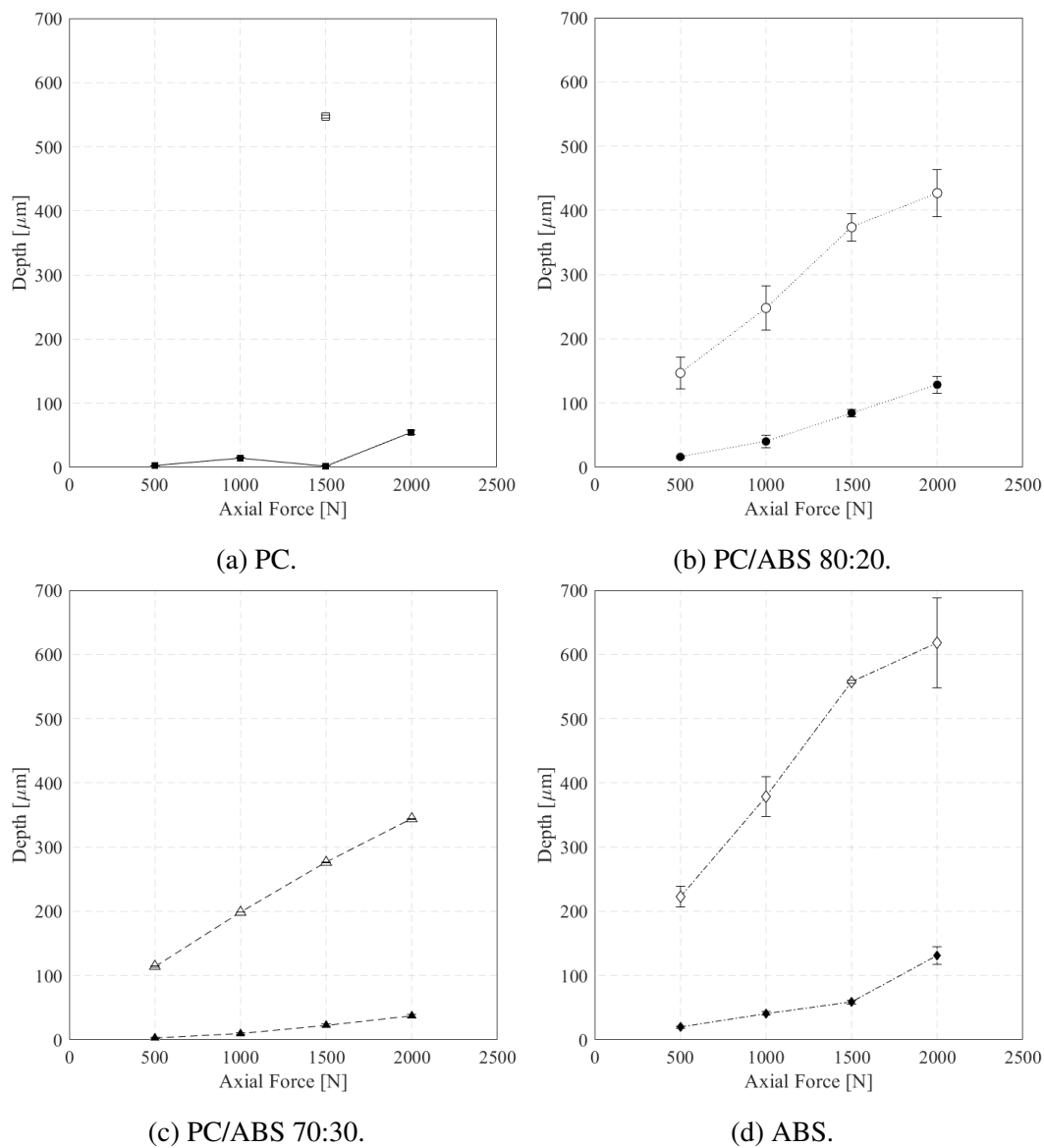


Figure 4.9: Indentation displacement (White) and averaged depth measurements(Black) .

From these results, the single value for in Fig. 4.9a shows the higher recovery, with the uncertain value obtained for 1500N. Apart from PC, ABS results in Fig. 4.9d indicates the higher recoveries for every load level. Results for both blends, shown in Figs. 4.9b and 4.9c presented the similar recoveries.

4.4 HARDNESS RESULTS

These testing methods were chosen due to equipment availability, our study group is heavily focused in the study of metallic materials and so are the current testing machines, but also to evaluate the hardness in different size scales and compare the obtained results with previous studies using another PC/ABS blend. The average values for micro-Vickers hardness (HV 0.1) and Brinell hardness (HBW 2.5/300) are presented in Tab. 4.3.

Table 4.3: Average standardized hardness of the specimens.

| Material | HV 0.1 | HBW 2.5/300 |
|---------------------|----------------|--------------------|
| PC | 14.5 ± 1.2 | 16.0 ± 0.7 |
| PC/ABS 80:20 | 13.2 ± 0.2 | 13.5 ± 0.3 |
| PC/ABS 70:30 | 16.6 ± 1.2 | 15.9 ± 0.3 |
| ABS | 12.1 ± 0.4 | 13.7 ± 0.2 |

Overall, results showed small variation among materials and although similar for both methods, they should not be directly compared since test conditions and methods were different. Besides the general similarity, ABS shows lower values for both tests as expected but PC does not present the higher values, being lower than 70:30 for micro-Vickers and practically the same for Brinell. As for the blends, there is a great variation in hardness for a small difference of the blending ratios and values obtained for 80:20 are closer to ABS than PC.

On the contrary of the obtained results, studies on PC/ABS blends reported hardness variation within blend compositions, directly related with blending ratios. Krache R. and Debbah I. [59] investigated mechanical and thermal properties of these blends, they showed hardness variation with two distinct horizontal regions: one for matrices containing more ABS and other for the matrices rich in PC. This behavior is explained by the phase inversion of PC, which evolve from a dispersed to a continuous phase when its concentration is greater than 50%.

While unexpected, the behavior observed for the results in the current study can arise from the fact that materials came from different manufacturers, meaning that not only the blends might be manufactured using different PC and ABS but also that the tested materials might not be the same used in these blends. Unfortunately the datasheet provided by the manufacturers do not identify the materials, besides the commercial resin name, or provide the blending ratios.

Analyzing the standard deviations, the maximum value observed from the 12 measurements taken for HV and HB were, respectively 8.1% and 4.4%. This indicates a general homogeneity, for both macro and micro scales, throughout the surfaces of the tested samples of the same materials.

In order to further evaluate the scale effect on hardness an approximation might be obtained from the indentation measurements, presented in the previous section using Eq. (2.6),

but it can't be considered an actual Brinell hardness number. Factors such as the indenter surface finish, geometry deviations and insufficient specimen thickness, among others, implies in great limitations and compromises obtained values. Results for the standardized methods and Brinell approximations are presented in Fig. 4.10.

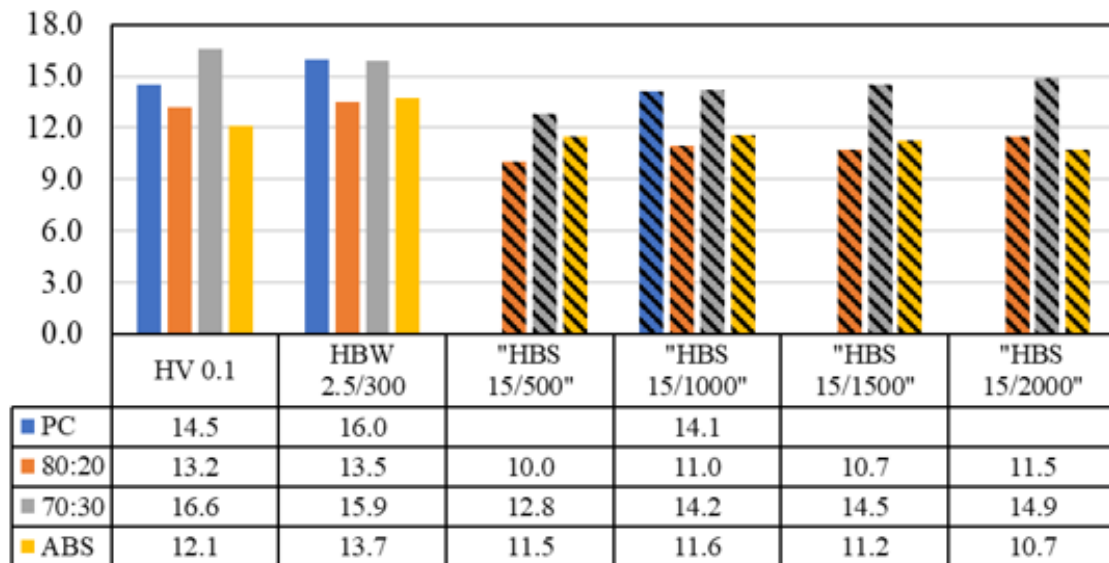


Figure 4.10: Standardized (Solid) and approximate hardness results (Diagonal stripes).

From the bar plot, the higher variations of hardness across micro and macro scales becomes more evident for PC and ABS, when compared with the blends, apart from being different test methods the increase of hardness was expected for all materials. This behavior is clearly present comparing the standard Brinell hardness with the approximations, indicating the effect of the increased indentator diameter resulting in lower hardness values, which is described not only in scientific studies but also at the standard method for Rockwell hardness of plastics - ASTM D785-03.

Comparing the approximation results for the three materials with values for all load levels, 70:30 presents a clear increase of hardness as load increases, 80:20 have a subtle increase and ABS shows similar values for 500N and 1000N, which decreases for the loads of the tests compromised by the insufficient specimen thickness.

4.5 UNCERTAINTIES

Applying the methodology previously presented to the results and equipment specifications, an uncertainty analysis was carried out to quantify the identified sources and investigate the which ones were the most relevant. Results are presented in three subsections, they are: 1. Load, 2. Indentation Diameter and 3. Indentation Depth.

4.5.1 LOAD

Composing load uncertainty the identified sources were: load transducer, static testing machine and data noise. For the load transducer the specifications from the manufacturer resulted in values shown in Tab. 4.4. All contributors were based on the 5000N capacity, but in low percentages, the combined uncertainty for this device is only 4.9N.

Table 4.4: Load transducer combined uncertainty and components.

| U_{hys} [N] | U_r [N] | U_{nl} [N] | CU_{lt} [N] |
|----------------------------|--------------------------|---------------------------|----------------------------|
| 2.5 | 1.5 | 4 | 4.9 |

The uncorrected error (U_{ue}), presented in Tab. 3.1, and estimated repeatability uncertainty (U_{res}), estimated following the calculation procedure described at ISO 7500-1, were combined into the static testing machine uncertainty (CU_{stm}) and values are presented in Tab. 4.5.

Table 4.5: Static testing machine combined uncertainty and components.

| Load [N] | U_{ue} [N] | U_{rep} [N] | CU_{stm} [N] |
|-----------------|---------------------------|----------------------------|-----------------------------|
| -500 | 1.3 | 0.7 | 1.5 |
| -1000 | 2.1 | 0.6 | 2.2 |
| -1500 | 3.2 | 0.2 | 3.2 |
| -2000 | 3.2 | 1.7 | 3.6 |

The resolution uncertainty (U_{res}), originated from the noise in the collected data showed great variation, as the histogram in Fig. 4.11 indicates, and although it presented a random behavior the higher registered value was considered to compose the load combined uncertainty.

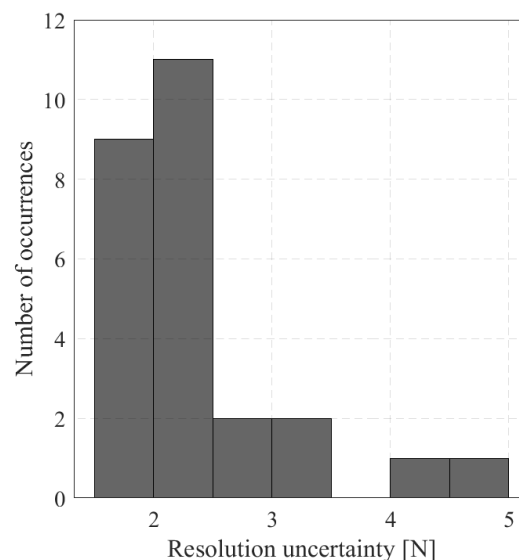


Figure 4.11: Resolution uncertainty histogram.

Table 4.6 shows the results for the load combined uncertainty (CU_{load}) and reveals that other contributors presented values inferior to the load transducer combined uncertainty, being the most relevant source, which in the worst case represented approximately 1% of the nominal load. Other contributors, like the uncorrected error or resolution, might be corrected through calibration procedures but the load transducer is an intrinsic component of the test machine and so is its uncertainties.

Table 4.6: Load combined uncertainties and components.

| Load [N] | CUlt [N] | CUstm [N] | Ures [N] | CUload [N] |
|--------------|----------|-----------|----------|------------|
| -500 | 4.9 | 1.5 | 4.6 | 6.9 |
| -1000 | 4.9 | 2.2 | 4.6 | 7.1 |
| -1500 | 4.9 | 3.2 | 4.6 | 7.4 |
| -2000 | 4.9 | 3.6 | 4.6 | 7.6 |

From the obtained results there is no evidence indicating that the test setup is not able to perform reliable experiments as proposed. The test machine was designed for high performance, its great accuracy is guaranteed through periodic and specialized maintenance and assured by calibration procedures.

4.5.2 INDENTATION DIAMETER

The indentation impression diameter measurements showed small variations among samples and directions that they were taken. Table 4.7 presents the averaged value along with the standard deviation of the measurements (s) and the expanded uncertainty (EU_d).

Table 4.7: Average indentation diameters, standard deviation and expanded uncertainty.

| Material | Load [N] | Average [mm] | s [mm] | EUd [mm] |
|---------------------|----------|--------------|--------|----------|
| PC | 500 | 1.674 | 0.14 | 0.16 |
| | 1000 | 2.942 | 0.03 | 0.16 |
| | 1500 | 3.686 | 0.05 | 0.20 |
| | 2000 | 4.039 | 0.02 | 0.22 |
| PC/ABS 80:20 | 500 | 2.536 | 0.10 | 0.17 |
| | 1000 | 3.421 | 0.11 | 0.21 |
| | 1500 | 4.223 | 0.03 | 0.23 |
| | 2000 | 4.686 | 0.14 | 0.29 |
| PC/ABS 70:30 | 500 | 2.243 | 0.14 | 0.19 |
| | 1000 | 3.009 | 0.02 | 0.16 |
| | 1500 | 3.637 | 0.03 | 0.20 |
| | 2000 | 4.132 | 0.04 | 0.23 |
| ABS | 500 | 2.367 | 0.04 | 0.13 |
| | 1000 | 3.327 | 0.03 | 0.18 |
| | 1500 | 4.123 | 0.02 | 0.22 |
| | 2000 | 4.862 | 0.05 | 0.27 |

Standard deviation values were considerably small, remaining in decimals of mm at most,

indicating great accuracy of the averaged measurements. The expanded uncertainty was always greater than the standard deviation. The maximum EU_d is approximately double the deviation for the same condition but in some cases, like 1500N ABS, it was 11 times greater. Relatively to the average, the highest uncertainty occurred for 70:30 at 500N, representing 8.5%.

In order to identify the greatest contributor for the diameter combined uncertainty (CU_d) Tab. 4.8 contains the estimated values for both standard uncertainty of the average (U_{std}) and confocal combined uncertainty (CU_{con}). The U_{std} ranged from 0.01 to 0.07mm while CU_{con} varies between 0.6-0.13 mm. As the standard deviation was small, so was its uncertainty, placing the confocal combined uncertainty as the most relevant contributor for the diameter, and the microscope as the major source of uncertainty.

Table 4.8: Indentation diameter combined uncertainty and components.

| Material | Load [N] | Ustd [mm] | CUcon [mm] | CUd [mm] |
|--------------|----------|-----------|------------|----------|
| PC | 500 | 0.07 | 0.05 | 0.08 |
| | 1000 | 0.02 | 0.08 | 0.08 |
| | 1500 | 0.02 | 0.10 | 0.10 |
| | 2000 | 0.01 | 0.11 | 0.11 |
| PC/ABS 80:20 | 500 | 0.05 | 0.07 | 0.08 |
| | 1000 | 0.05 | 0.09 | 0.11 |
| | 1500 | 0.01 | 0.11 | 0.11 |
| | 2000 | 0.07 | 0.13 | 0.14 |
| PC/ABS 70:30 | 500 | 0.07 | 0.06 | 0.09 |
| | 1000 | 0.01 | 0.08 | 0.08 |
| | 1500 | 0.02 | 0.10 | 0.10 |
| | 2000 | 0.02 | 0.11 | 0.11 |
| ABS | 500 | 0.02 | 0.06 | 0.07 |
| | 1000 | 0.02 | 0.09 | 0.09 |
| | 1500 | 0.01 | 0.11 | 0.11 |
| | 2000 | 0.02 | 0.13 | 0.13 |

Table 4.9 presenting the uncertainties related to the microscope accuracy and its measurement tool indicates that measurement tool was the highest uncertainty contributor, with values were comparable to the standard deviation previously presented. Overall uncertainty results for the diameter were coherent and small, indicating that its measurement procedure and equipment used were adequate.

4.5.3 INDENTATION DEPTH

As previously mentioned the expanded uncertainty for depth averages showed inconsistency. Table 4.10 shows the average values along with the standard deviation and the estimated uncertainty. From these results its noticeable that although the standard deviation (s) was smaller than expanded uncertainty (EU_h) for all configurations, they present great correlation.

Table 4.9: Combined confocal uncertainty and components for indentation diameter.

| Material | Load [N] | Uacc [mm] | Umt [mm] | CUcon [mm] |
|---------------------|-----------------|------------------|-----------------|-------------------|
| PC | 500 | 0.02 | 0.04 | 0.05 |
| | 1000 | 0.03 | 0.07 | 0.08 |
| | 1500 | 0.04 | 0.09 | 0.10 |
| | 2000 | 0.04 | 0.10 | 0.11 |
| PC/ABS 80:20 | 500 | 0.03 | 0.06 | 0.07 |
| | 1000 | 0.03 | 0.09 | 0.09 |
| | 1500 | 0.04 | 0.11 | 0.11 |
| | 2000 | 0.05 | 0.12 | 0.13 |
| PC/ABS 70:30 | 500 | 0.02 | 0.06 | 0.06 |
| | 1000 | 0.03 | 0.08 | 0.08 |
| | 1500 | 0.04 | 0.09 | 0.10 |
| | 2000 | 0.04 | 0.10 | 0.11 |
| ABS | 500 | 0.02 | 0.06 | 0.06 |
| | 1000 | 0.03 | 0.08 | 0.09 |
| | 1500 | 0.04 | 0.10 | 0.11 |
| | 2000 | 0.05 | 0.12 | 0.13 |

Table 4.10: Average indentation depth, standard deviation and expanded uncertainty.

| Material | Load [N] | Average [μm] | s [μm] | EUh [μm] |
|---------------------|-----------------|-------------------------------------|-------------------------------|---------------------------------|
| PC | 500 | 2.330 | 0.57 | 0.62 |
| | 1000 | 14.644 | 0.22 | 0.84 |
| | 1500 | 1.950 | 0.44 | 0.50 |
| | 2000 | 54.461 | 2.56 | 3.81 |
| PC/ABS 80:20 | 500 | 16.102 | 1.74 | 1.95 |
| | 1000 | 40.145 | 9.33 | 9.57 |
| | 1500 | 84.628 | 3.78 | 5.77 |
| | 2000 | 128.488 | 11.65 | 13.39 |
| PC/ABS 70:30 | 500 | 2.981 | 0.72 | 0.77 |
| | 1000 | 9.612 | 1.35 | 1.47 |
| | 1500 | 22.732 | 0.62 | 1.37 |
| | 2000 | 37.406 | 0.53 | 2.03 |
| ABS | 500 | 19.993 | 1.31 | 1.70 |
| | 1000 | 41.131 | 2.24 | 3.11 |
| | 1500 | 58.686 | 0.54 | 3.09 |
| | 2000 | 131.291 | 11.83 | 13.63 |

Both PC and 70:30 at 500N had the two lowest uncertainties and average, but they represented approximately 26% of the average depth. In general both materials had the smaller values, the low standard deviation shows that averaged measurements were similar. These two factors, in addition to the confocal uncertainties being directly related to the measured dimension, induced smaller uncertainties.

The disperse load-displacement curves obtained for 80:20 and ABS caused a major variation in the displacement and their depth results reflects that trough the standard deviation. This becomes very clear looking at ABS results for 1500N, this configuration showed the

smaller deviation and uncertainty representing, respectively, 0.9% and 5.3% of the average. On the other hand results for 80:20 at 1000N evidence the problem, with deviation and uncertainty equivalent to 23.2% and 23.8% of the average depth.

Table 4.11: Indentation depth combined uncertainty and components.

| Material | Load [N] | Ustd [μm] | CUcon [μm] | CUh [μm] |
|--------------|----------|------------------|-------------------|-----------------|
| PC | 500 | 0.28 | 0.13 | 0.31 |
| | 1000 | 0.11 | 0.41 | 0.42 |
| | 1500 | 0.22 | 0.12 | 0.25 |
| | 2000 | 1.28 | 1.41 | 1.91 |
| PC/ABS 80:20 | 500 | 0.87 | 0.44 | 0.97 |
| | 1000 | 4.67 | 1.07 | 4.79 |
| | 1500 | 1.89 | 2.18 | 2.89 |
| | 2000 | 5.82 | 3.31 | 6.70 |
| PC/ABS 70:30 | 500 | 0.36 | 0.14 | 0.38 |
| | 1000 | 0.68 | 0.28 | 0.73 |
| | 1500 | 0.31 | 0.61 | 0.68 |
| | 2000 | 0.27 | 0.98 | 1.01 |
| ABS | 500 | 0.65 | 0.54 | 0.85 |
| | 1000 | 1.12 | 1.07 | 1.55 |
| | 1500 | 0.27 | 1.52 | 1.54 |
| | 2000 | 5.92 | 3.38 | 6.81 |

In order to unravel the expanded uncertainty Tab. 4.11 contains the estimated values for the combined uncertainty and its components. As expected the confocal uncertainties followed the ascending measurements, while the standard uncertainty of the mean shows very different values. Comparing the uncertainties of the mentioned configurations, the U_{std} was more than four times greater than CU_{con} for 80:20 at 1000N while for ABS at 1500N this difference is only 17.8%, placing the measurement values as most relevant source of uncertainty.

To examine the contribution of the accuracy and the measurement tool for the confocal combined uncertainty, values are presented in Tab. 4.12. With the exception of PC and 70:30 at 500N, which had the two lowest depths, presented higher values of U_{mt} than U_{acc} and its due to the accuracy being defined as a constant added to a percentage of the dimension taken.

Besides the mentioned configuration the combined uncertainty remained between 5.1-5.9% of the average depth, this indicates that the measurement tool uncertainty, assumed as 5% of the dimension, was the major contributor for the microscope uncertainty.

Considering a scenario with no standard uncertainty of the mean the EU_h would be $2 \times CU_{con}$. Taking ABS at 1500N and 80:20 at 1000N as examples their expanded uncertainty would go, respectively, from $3.09\mu m$ and $9.57\mu m$ to $3.4\mu m$ and $2.14\mu m$. In this new scenario the depth uncertainty for 80:20 would correspond to 22.3% of its actual value

Table 4.12: Combined confocal uncertainty and components for indentation depth.

| Material | Load [N] | Uacc [μm] | Umt [μm] | CUcon [μm] |
|--------------|----------|------------------|-----------------|-------------------|
| PC | 500 | 0.11 | 0.06 | 0.13 |
| | 1000 | 0.17 | 0.37 | 0.41 |
| | 1500 | 0.11 | 0.05 | 0.12 |
| | 2000 | 0.37 | 1.36 | 1.41 |
| PC/ABS 80:20 | 500 | 0.18 | 0.40 | 0.44 |
| | 1000 | 0.30 | 1.02 | 1.07 |
| | 1500 | 0.52 | 2.12 | 2.18 |
| | 2000 | 0.74 | 3.22 | 3.31 |
| PC/ABS 70:30 | 500 | 0.11 | 0.08 | 0.14 |
| | 1000 | 0.15 | 0.24 | 0.28 |
| | 1500 | 0.21 | 0.57 | 0.61 |
| | 2000 | 0.29 | 0.94 | 0.98 |
| ABS | 500 | 0.20 | 0.50 | 0.54 |
| | 1000 | 0.31 | 1.03 | 1.07 |
| | 1500 | 0.39 | 1.47 | 1.52 |
| | 2000 | 0.76 | 3.29 | 3.38 |

4.6 AVERAGE MATERIAL BEHAVIOR

4.6.1 REGRESSION CURVES

In order to obtain the average material behavior from the collected data, all files from the same material were concatenated and a regression with a second order polynomial model was applied, using the relation:

$$y = c_2x^2 + c_1x \quad (4.1)$$

This model was chosen not only for its simplicity, but also because was the best linear model to represent the curves obtained for the different materials. Plots with the experimental data, regression curve and uncertainty envelope are presented in Figs. 4.12,4.13,4.14 and 4.15, including the obtained equation, R^2 and the regression root-mean-square error (*rmse*).

Both curves captured for PC shown in Fig. 4.12 were very similar, showing practically no deviation, which resulted in the higher R^2 and lower regression error with the value of 15.6N. Due to the major dispersion of the curves for PC/ABS 80:20 the obtained regression, presented in Fig. 4.13, the regression error was the higher observed with the value of 104.1N.

Along with the results for PC, the blend 70:30 also presented great accordance among curves and a good fit with the proposed regression, shown in Fig. 4.14, which have the second higher R^2 with the value of 0.998 and the second lower error with $rmse = 24.3N$.

The variability of ABS results, shown in Fig. 4.15 provided a regression that ended up masking the observed change of curve behavior due to lack of specimen thickness. This

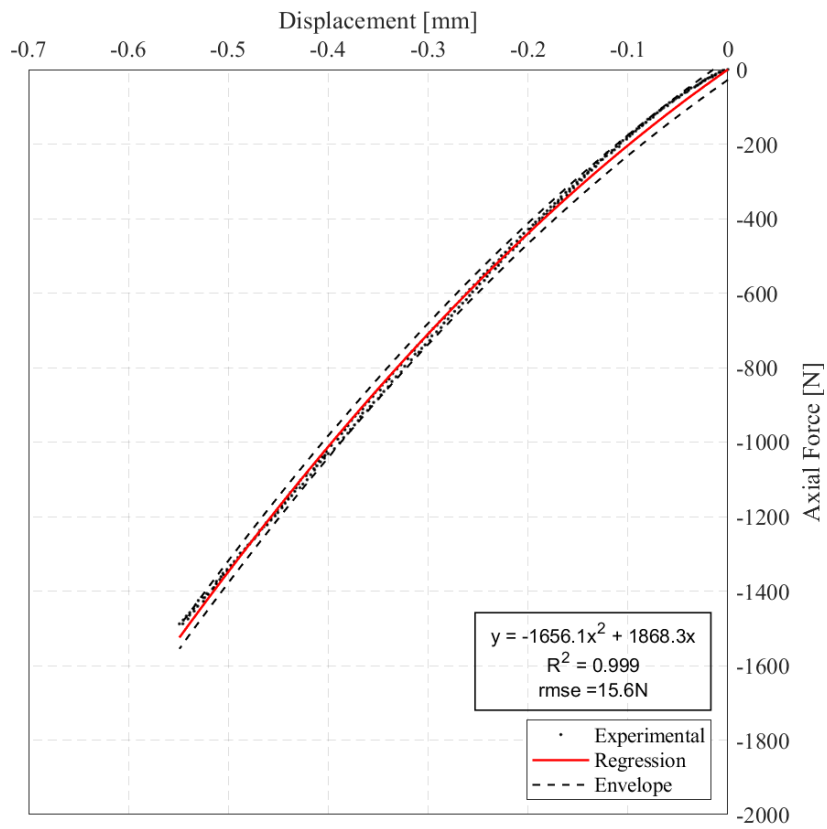


Figure 4.12: Load-displacement regression for tests on PC.

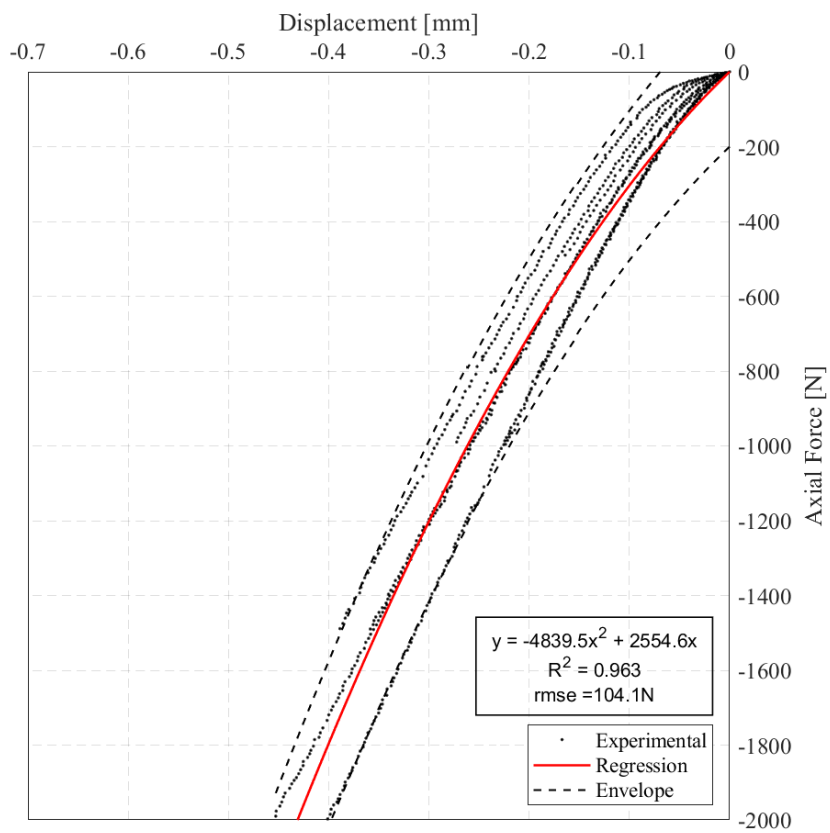


Figure 4.13: Load-displacement regression for tests on PC/ABS 80:20.

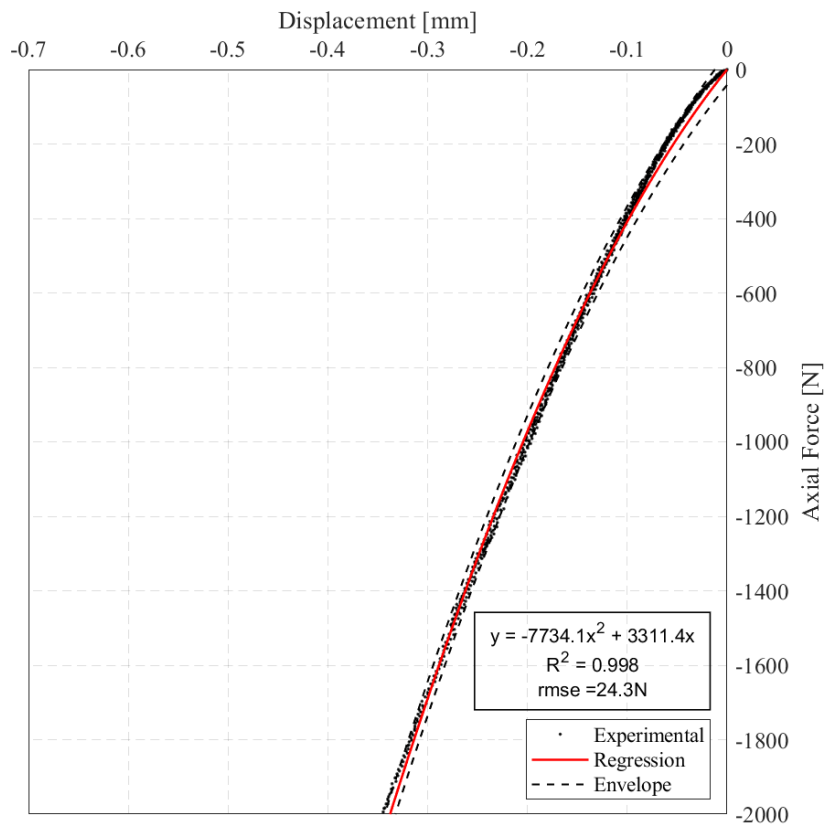


Figure 4.14: Load-displacement regression for tests on PC/ABS 70:30.

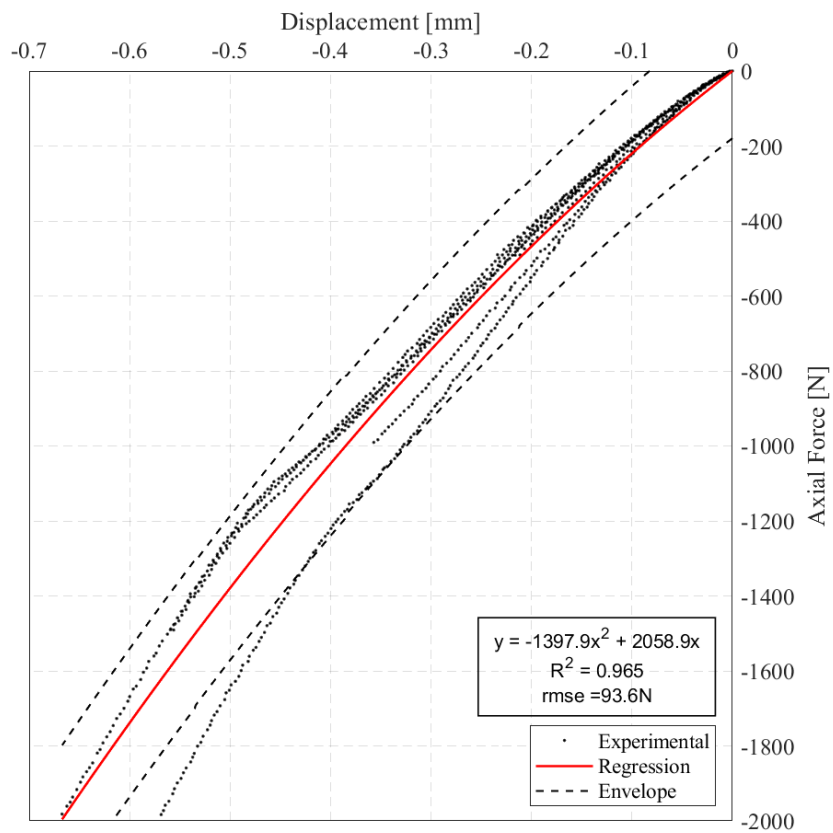


Figure 4.15: Load-displacement regression for tests on ABS.

compromise the use of the obtained regression curve for comparison to future experiments. On the other hand this results raised a flag on load/thickness relationship, providing the first step of a future investigation.

Overall, the obtained regressions were satisfactory. The high values of R^2 are due to the elevated number of data points, which ended up masking the quality of the regressions, and a residual analysis was carried out.

4.6.2 RESIDUALS ANALYSIS

In order to further analyze the obtained regressions Tab. 4.13 presents regressions R^2 and root-mean-square error ($rmse$), and the coverage factor (k) and the maximum value for the uncertainty envelopes.

Table 4.13: Regression outputs and envelope key values.

| Material | R^2 | $rmse$ [N] | k | Max bound [N] |
|--------------|-------|------------|-----|---------------|
| PC | 0.999 | 15.6 | 4 | 30.4 |
| PC/ABS 80:20 | 0.963 | 104.1 | 29 | 220.4 |
| PC/ABS 70:30 | 0.998 | 24.3 | 6 | 45.6 |
| ABS | 0.965 | 93.6 | 26 | 197.6 |

The $rmse$ value was not obtained directly from the goodness of fit of the regressions due to the high concentration of the residuals at specific zones, to minimize this effect they were calculated for each load level, allowing a comparison with the local combined uncertainty. The uncertainty envelope was attained using the concept of expanded uncertainty. From the complete regression array, the higher 5% values were eliminated and the maximum value was divided by the combined uncertainty of that load range, providing the coverage factor that expands the uncertainty with 95% confidence.

The maximum load combined uncertainty (CU_{load}) of 7.6N from Tab. 4.6 was at least half of the minimum $rmse$, which was considerable low due to the elevated number of data points. For that reason, the coverage factor to define the uncertainty envelope varied between 4 and 29, resulting in maximum values of the envelope between 30.4-220.4N. This indicators translates into numbers the major variability seen in the load-displacement curves for some of tested materials.

Figure 4.16 provides a visualization of these indicators compared with the actual residuals. As expected, the residuals for PC and PC/ABS 70:30, respectively in Figs. 4.16a and 4.16c, shows that regressions are capable to represent the average behavior even though $k > 2$, which is the usual value to have EU with 95% confidence.

The residuals for PC/ABS 80:20 presented in Fig. 4.16b shows not only high residuals, but the spikes that arises from divergence from the regression and the end of each test curves are dislocated due to the dispersion of the curves when consolidated, requiring the higher envelope values.

Residuals for the ABS regression, show in Fig. 4.16d, had the higher values, reaching up to 380N, but as they were concentrated in a single spike the required envelope was smaller than for the 80:20 blend. This spike is also at the zone which the curves had a change in behavior, revealing how greatly this event was suppressed by the regression applied.

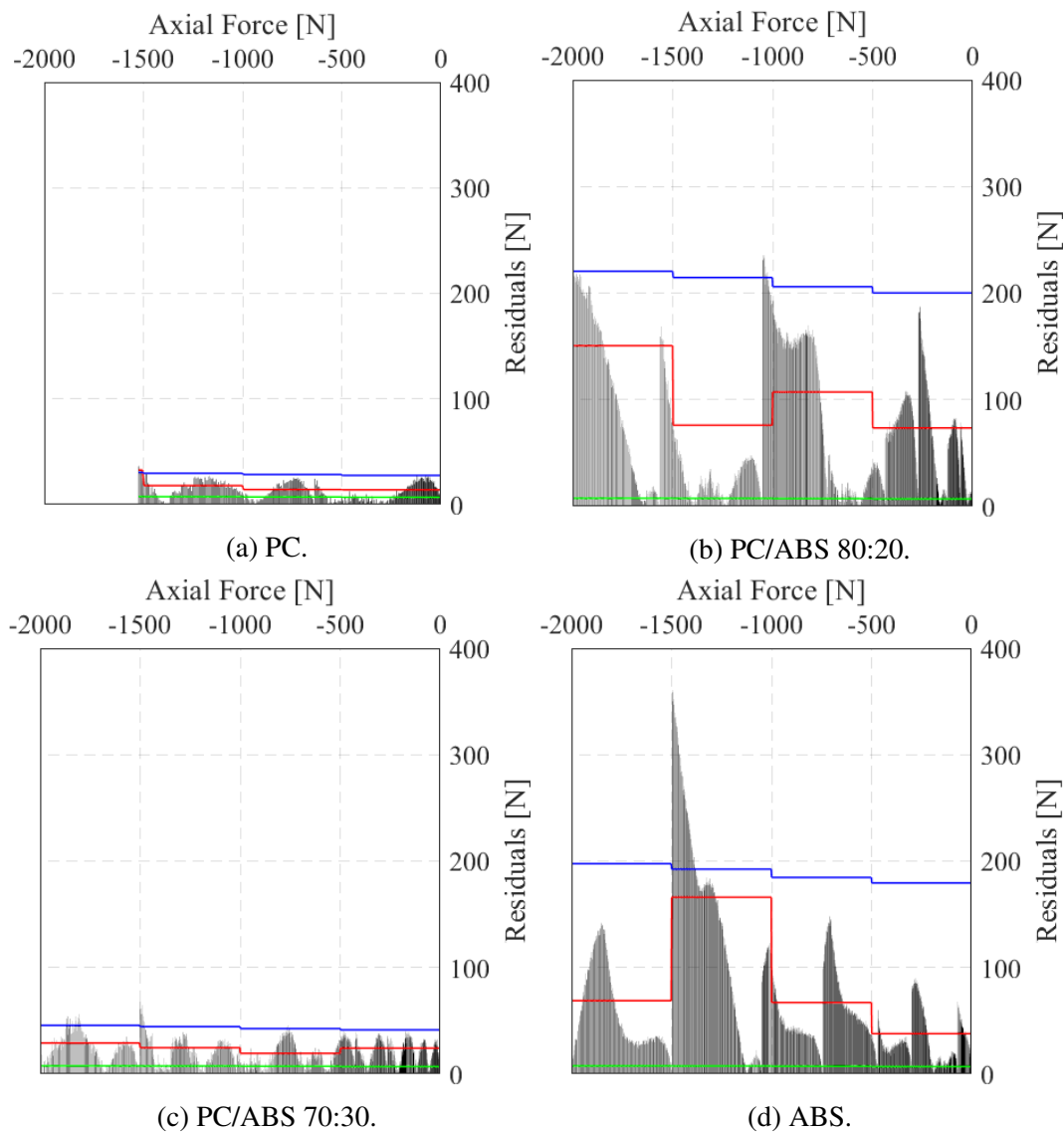


Figure 4.16: Load vs regression residuals (Green: CU_{load} , Red: $rm.se$ and Blue: Envelope).

The high residuals values demonstrates that either the collected data was in a certain way compromised by flaws in the methodology or, since hardness results indicated surface homogeneity, the tested samples might present considerable internal differences. Even though samples of each material came from the same batch, the lack of information on their manufacture process don't allow us to discard this possibility until they are further analyzed.

Chapter 5

FINAL REMARKS

5.1 CONCLUSIONS

This work was based on sphere-to-flat indentation tests of four different polymers, being PC, ABS and two PC/ABS blends in the ratios of 80:20 and 70:30. Tests were performed in a MTS Landmark® testing machine, using a custom sample holder device, at four load levels: 500N, 1000N, 1500N and 2000N. Results were obtained from load-displacement curves collected during indentation, post-test microscopic analysis and a thorough multi-uncertainty analysis.

Based on the equipment used in the process three of them contained uncertainty sources related to the load readings, indentation depth and indentation diameter. Altogether, ten different uncertainty contributors were identified and quantified in order to point out the most relevant contributions to the uncertainty of the three variables of interest.

The load presented approximately 1% of the nominal load as combined uncertainty at the worst case, which was for 500N. The main contributors came from the load transducer, an essential device with no possible correction besides the substitution for another with lower full scale capacity.

Despite the resolution contributor, due to the noise amplitude in the collected data, all other components were identical for each load level, resulting in similar uncertainty values. The high values for the coverage factor, necessary to obtain the uncertainty envelope through expansion, indicates that there is significant material or methodology inconsistencies affecting test results.

All load-displacement curves collected were analyzed and had their corresponding uncertainties quantified. From this data the average behavior of the studied materials was obtained using a regression model and an uncertainty envelope was generated as well.

Three contrasting scenarios were observed:

1. Consistent data: Curves for PC and PC/ABS 70:30 were very consistent among the

different tests, both presented the lowest regression residuals and standard error;

2. Inconsistent data: All tests performed on PC/ABS 80:20 and ABS tests at 500N and 1000N had great variation in the results, resulting in a regression with higher residuals and standard errors;
3. Compromised data: Tests on ABS samples with loads of 1500 and 2000N were compromised by the specimen thickness, showing marks on the opposite surface of the indentation marks, corroborating the idea of ABS being the most ductile material in the study and raising awareness to the relation of the thickness and applied load.

The indentation diameter measurements were consistent, evidenced by the small standard deviation, and so were their expanded uncertainty which reaches a maximum value of 8.5% of the average value, arising from the confocal microscope.

On the indentation depth there was a significant difference in results. Measurements taken were considerably different for the same configurations, noticeable due to the inconsistent standard deviation and expanded uncertainty values. The major contributor in this case were the measurements obtained, not due to the microscope but from the impression geometry itself due to unclear effects from inconsistencies related to: repeatability, during sample preparation and test methodology, or the materials. The expanded uncertainty represented up to 20% of the indentation depth in three different configurations, two of them were due to the undermost obtained average while for PC/ABS 80:20 it happened due to the difference of the measurements.

5.2 FUTURE WORKS

Overall, the equipment available was suitable for the experiments and marks analysis. Nevertheless, for future studies adjustments are necessary to the repeatability and methodology problems, they are focused on the indenter, sample holder device, samples and test procedure.

As indicated in the standards related to hardness tests, the indenter shall have a polished surface finish, be free of defects and have a small deviation. Due to the issue identified through the ABS tests the device must be able to accommodate samples with thickness greater than 6mm, for future tests using loads higher than 1000N on these polymeric materials. Once the load levels of future studies are defined, a thorough evaluation of the thickness/load relation must be performed, determining the new specimen geometries.

The following recommendations are made for the future methodology:

- At least five indentation tests for each configuration;
- Run tests with displacement control and load interlock instead of load control;

- Either start the test without gap or with a standardized one;
- Also record the load-displacement curve during the loading removal phase.

The recommendation of running tests with displacement limits intends to create uniform data sets for each test, facilitating the analysis and also allowing the uncertainty evaluation of the regression model. By doing so the envelope might be represented by the experimental uncertainty of the load combined with the uncertainty of the regression model, including the uncertainty of the coefficients, thus allowing prediction models to be created for the material behavior.

In order to do so, it is also important to quantify not only the uncertainty of the LVDT for the intended displacement but also the sensitivity of the device, assuring that really small variations are captured in order to avoid exceeding the capacity of the load transducer.

All uncertainty related to the samples and materials being testes must be removed, most importantly if future studies are focused on the mechanical characterization of the different blending ratios. In order to do so, the following suggestions are made:

- Produce the different blends samples using the same PC and ABS in study;
- Obtain the elastic and plastic properties of the materials under compression;
- Control blending ratios through mass and volume of the components;
- Reduce dimensional variability;
- Control the manufacturing process of the samples, using ASTM D3641-02 as reference;
- Eliminate manufacture errors;
- Improve sample preparation and quality control.

REFERENCES

- [1] HOME | Codeplas. <http://www.codeplas.pt/en>. Acesso em: 02/02/2021.
- [2] DOCA, T.; PIRES, F. M. A. Experimental and numerical analysis of the surface properties of the pc/abs. New York, 2018.
- [3] PANDIM, T. *Torsional fretting wear experimental analysis of a R3 offshore steel against a PC/ABS blend*. [S.l.]: University of Brasilia, 2019.
- [4] PANDIM, T. et al. Torsional fretting wear experimental analysis of a r3 offshore steel against a pc/abs blend. *Tribology International*, Elsevier, n. 143, p. 1–10, 9 2019.
- [5] LINS, G.; LORENZO, T. *Projeto de dispositivo para ensaios de contato entre sólidos com geometria hertziana*. [S.l.]: University of Brasilia, 2017.
- [6] PLASTICS, M.; HARPER, C. *Modern Plastics Handbook*. New York, United States: McGraw-Hill, 2000.
- [7] UTRACKI, L.; WILKIE, C. *Polymer Blends Handbook*. [S.l.: s.n.], 2014. 1-2378 p. ISBN 978-94-007-6063-9.
- [8] PLASTICS - the facts 2019. <https://www.plasticseurope.org/en/resources/publications/1804-plastics-facts-2019>. Acesso em: 20/04/2020.
- [9] CHANDA, M.; ROY, S. *Industrial Polymers, Specialty Polymers, and Their Applications*. [S.l.: s.n.], 2008. 1-405 p. ISBN 9780429140631.
- [10] HARPER, C.; PETRIE, E. *Plastic Materials and Processes: A Concise Encyclopedia*. New Jersey, United States: Wiley-Interscience, 2003.
- [11] HOURSTON, D. Alloys and blends. In: SWALLOWE, G. (Ed.). *Mechanical Properties and Testing of Polymers*. [S.l.]: Springer Netherlands, 1999, (Polymer Science and Technology Series, 1). p. 20–22.
- [12] GRECO, R.; DONG, L. Pc/abs blends: Compatibilization and mechanical behaviour. *Macromolecular Symposia*, v. 78, p. 141 – 153, 02 1994.
- [13] JOHNSON, K. L. *Contact Mechanics*. [S.l.]: Cambridge University Press, 1985.

- [14] DOWLING, N. E. (Ed.). *Mechanical Behavior of Materials*. 4. ed. United Kingdom: Pearson Education, 2013.
- [15] SETH, B. R. Transition theory of elastic-plastic deformation, creep and relaxation. *Nature International Journal of Science*, Nature Publishing Group, n. 4844, p. 896–897, 9 1962.
- [16] HAWARD, R. N.; YOUNG, R. J. The physics of glassy polymers. In: _____. 2. ed. United Kingdom: Springer, 1997. cap. 1, p. 1–29.
- [17] CLARKE, J. H. R. The physics of glassy polymers. In: _____. 2. ed. United Kingdom: Springer, 1997. cap. 2, p. 33–82.
- [18] MECHANICAL Testing of Polymers and Ceramics. In: ASM Handbook. [S.l.]: ASM International, 2000. v. 8.
- [19] BILLMEYER, F. *Textbook of Polymer Science*. 3. ed. [S.l.]: Wiley-Interscience, 1984.
- [20] HUTCHINSON, J. M. The physics of glassy polymers. In: _____. 2. ed. United Kingdom: Springer, 1997. cap. 3, p. 85–155.
- [21] CRIST, B. The physics of glassy polymers. In: _____. 2. ed. United Kingdom: Springer, 1997. cap. 4, p. 155–210.
- [22] GAUTHIER, C. Non elastic deformation during a mechanical test. In: SWALLOWE, G. (Ed.). *Mechanical Properties and Testing of Polymers*. [S.l.]: Springer Netherlands, 1999, (Polymer Science and Technology Series, 1). p. 174–178.
- [23] SCHÜMANN, K. et al. Conversion of engineering stresses to cauchy stresses in tensile and compression tests of thermoplastic polymers. *Current Directions in Biomedical Engineering*, v. 2, p. 649–652, 09 2016.
- [24] BOYCE, M. C.; HAWARD, R. N. The physics of glassy polymers. In: _____. 2. ed. United Kingdom: Springer, 1997. cap. 5, p. 213–289.
- [25] DONALD, A. M. The physics of glassy polymers. In: _____. 2. ed. United Kingdom: Springer, 1997. cap. 6, p. 295–339.
- [26] CHUI, C.; BOYCE, M. Monte carlo techniques applied to polymer deformation. In: SWALLOWE, G. (Ed.). *Mechanical Properties and Testing of Polymers*. [S.l.]: Springer Netherlands, 1999, (Polymer Science and Technology Series, 1).
- [27] ASTM E9-19 - Standard Test Methods of Compression Testing of Metallic Materials at Room Temperature. Pennsylvania, United States, 2019.
- [28] COMPRESSION Test. Disponível em: <<https://www.ultrac.com/en/solutions/test-methods/mechanical/compression-test.html>>. Acesso em: 13/01/2021.

- [29] Hardness testing. In: CHANDLER, H. (Ed.). 2. ed. New Jersey, United States: ASM International, 1999. cap. 1, p. 1–14.
- [30] TABOR, D. The hardness of solids. *Review of Physics in Technology*, v. 1, p. 145–179, 11 1970.
- [31] SPARY, I.; BUSHBY, A.; JENNETT, N. On the indentation size effect in spherical indentation. *Philosophical Magazine*, v. 86, p. 5581–5593, 11 2006.
- [32] SWADENER, J.; GEORGE, E.; PHARR", G. The correlation of the indentation size effect measured with indenters of various shapes. *Journal of the Mechanics and Physics of Solids*, v. 50, n. 4, p. 681 – 694, 2002. ISSN 0022-5096.
- [33] PHARR, G.; HERBERT, E.; GAO, Y. The indentation size effect: A critical examination of experimental observations and mechanistic interpretations. *Annual Review of Materials Research*, v. 40, p. 271–292, 07 2010.
- [34] GOULDSTONE, A. et al. Indentation across size scales and disciplines: Recent developments in experimentation and modeling. *Acta Materialia*, v. 55, n. 12, p. 4015 – 4039, 2007. ISSN 1359-6454.
- [35] BRISCOE, B. J.; SHINHA, S. K. Hardness and normal indentation of polymers. In: SWALLOWE, G. (Ed.). *Mechanical Properties and Testing of Polymers*. [S.l.]: Springer Netherlands, 1999, (Polymer Science and Technology Series, 1). p. 113–122.
- [36] DRISCOLL, S. (Ed.). *The Basics of Testing Plastics: Mechanical Properties, Flame Exposure, and General Guidelines*. West Conshohocken, PA: ASTM International, 1998. (ASTM manual series; MNL 35).
- [37] ASTM D695-15 - Standard Test Method for Compressive Properties of Rigid Plastics. Pennsylvania, United States, 2015.
- [38] PLASTICS - Standard atmospheres for conditioning and testing. Geneva, Switzerland, 11 2005.
- [39] STANDARD Practice for Conditioning Plastics for Testing. Pennsylvania, United States, 2000.
- [40] BROWN, R. (Ed.). *Handbook of Polymer Testing*. [S.l.]: Rapra Technology, 2002. (Rapra Polymer Testing Series).
- [41] ASTM E10-00 - Standard Test Method for Brinell Hardness of Metallic Materials. Pennsylvania, United States, 2000.
- [42] ASTM D785-03 - Standard Test Method for Rockwell Hardness of Plastics and Electrical Insulating Materials. Pennsylvania, United States, 2003.

- [43] JCGM 100:2008 - Guia para a expressão de incerteza de medição. Brasil, 2008.
- [44] BELL, S. A beginner's guide to uncertainty measurement. In: *Measurement Good Practice Guide*. United Kingdom: National Physical Laboratory, 1999. p. 1–16.
- [45] DAHLBERG, G. Materials testing machines investigation of error sources and determination of measurement uncertainty. In: SATIR, A.; SENNHAUSER, W. (Ed.). *Investigation and Verification of Materials Testing Machines*. [S.l.]: EUROLAB, 2001.
- [46] SWALLOWE, G. Accuracy and errors. In: SWALLOWE, G. (Ed.). *Mechanical Properties and Testing of Polymers*. [S.l.]: Springer Netherlands, 1999, (Polymer Science and Technology Series, 1). p. 1–4.
- [47] MTS Landmark Testing Solutions. https://www.mts.com/cs/groups/public/documents/library/dev_004324.pdf. Acesso em: 23/12/2020.
- [48] MTS 661.19 Force Transducer. 1996. https://www.mts.com/cs/groups/public/documents/library/dev_003709.pdf. Acesso em: 23/12/2020.
- [49] LINS, G.; LORENZO, T.; DOCA, T. Design and manufacture of a sample holder device for fretting wear tests. In: *25th International Congress of Mechanical Engineering (COBEM) Proceedings*. [S.l.]: ABCM, 2019.
- [50] LEXT OLS4000 Industrial Laser Confocal Microscopes - Olympus 3D Laser Measuring Solution. <https://www.olympus-ims.com/pt/metrology/ols4000/>. Acesso em: 02/12/2020.
- [51] LEXAN Resin 243R. [S.l.], 2017.
- [52] NOVODUR Ultra 4140PG. [S.l.], 2016.
- [53] MABLEX PCA. [S.l.], 2010.
- [54] TERLURAN GP-35. [S.l.], 2016.
- [55] GRELLMANN, W.; SEIDLER, S. *Landolt-Börnstein Numerical Data and Functional Relationships in Science and Technology*. [S.l.]: Springer-Verlag, 2014. (A, v. 6).
- [56] MACHADO, L. *Extraction of Plasticity Parameters of Metallic Materials From Spherical Indentation Tests and FEM Modeling*. [S.l.]: University of Brasilia, 2019.
- [57] ASTM D3641-02 - Standard Practice for Injection Molding Test Specimens of Thermoplastic Molding and Extrusion Materials. Pennsylvania, United States, 2002.
- [58] METALLIC Materials - Verification of static uniaxial testing machines - Part 1: Tension/compression testing machines - Verification and calibration of the force-measuring system. 3. ed. Geneva, Switzerland, 2004.

[59] KRACHE, R.; ISMAHANE, D. Some mechanical and thermal properties of pc/abs blends. *Materials Sciences and Applications*, v. 2, p. 404–410, 01 2011.

APPENDIX I

Scan and measurement procedures - LEXT OLS4000 Confocal microscope

The procedural algorithm is a detailed version of the methodology presented in Sec. 3.2, covering the setup for the scanning process, items 1-23, along with the measurement procedure, items 24-33.

1. Verify if there is enough clearance between the lens and the base;
2. Turn on the computer and the microscope;
3. Launch the OLS 4000 software;
4. Position the sample below the optical lenses;
5. Starting with the 5X lenses, use your thumb to unlock the control wheel while holding it in place;
6. Adjust the Z position until a focused image is obtained;
7. Lock the control wheel in place;
8. Change the optical lenses and repeat the height adjustment until the desired magnification is achieved;
9. Adjust the brightness level to 50 and change it to obtain a clear image of the indentation mark, this setting depends on the material used and must be checked for each sample;
10. Align the field of view as closer to the center of the mark and, using the software control, adjust the height downwards until the focus is lost;
11. Change to the laser view and further decrease the height until there is no visible image, this will guarantee that the bottom is defined below the indentation mark depth (during this process be aware of the gap between the optical lens and the specimen's surface);
12. Define the bottom limit as the current position;
13. Change to the color view and increase the z position until focus is achieved again;

14. Move the field of view to the specimen surface, in a region unaffected by the indentation, and adjust the height to obtain a focused image;
15. For the top limit definition, repeat the procedure for the bottom definition in the opposite direction;
16. Return the field of view to the center of the indentation mark;
17. Check the Color option box to capture the image along with the scan;
18. Check the Step option and define the step height;
19. Click in Stitching
20. In the new window, check the option by number of pieces;
21. Define a value that, considering the chosen magnification, will be able to capture the full mark;
22. Define the base positioning at center and click to update reference, if necessary go to the small display and center;
23. Start the stitching process;
24. Once the process is finished, open the measurement environment;
25. Go to profile measurement;
26. Choose the X profile line and manually align the line in the image over the greater diameter;
27. Choose the measurement type with horizontal and vertical parallel lines;
28. Apply the surface correction;
29. Apply the Jagged surface noise filter to smooth the 2D profile;
30. Manually align the vertical lines with the diameter, using the blue/red indicator on the image as reference;
31. Manually align the horizontal lines with the top and bottom of the 2D profile;
32. Register the height and length measurements;
33. Save the image, using the sample ID and magnification applied in the image name, for documentation and future inspection if necessary.